Article

Precision Agriculture: Temporal and Spatial Modeling of Wheat Canopy Spectral Characteristics

Donghui Zhang [1], Liang Hou [2,*], Liangjie Lv [3], Hao Qi [2], Haifang Sun [2], Xinshi Zhang [2], Si Li [2], Jianan Min [2], Yanwen Liu [4], Yuanyuan Tang [5] and Yao Liao [6]

1   Institute of Remote Sensing Satellite, China Academy of Space Technology, Beijing 100094, China;
    zhangdonghui@alu.cdut.edu.cn
2   Institute of Agricultural Information and Economy, Hebei Academy of Agriculture and Forestry Sciences,
    Shijiazhuang 050051, China; njsqihao@163.com (H.Q.); njssenhifon@163.com (H.S.);
    zhangxinshi@126.com (X.Z.); wsls0224@163.com (S.L.); minjn2019@163.com (J.M.)
3   Institute of Cereal and Oil Crops, Hebei Academy of Agriculture and Forestry Sciences,
    Shijiazhuang 050035, China; liangjie_lv@163.com
4   School of Resources and Environment Science and Engineering, Hubei University of Science and Technology,
    Xianning 437100, China; lhgyanzi@whu.edu.cn
5   Changsha Natural Resources Comprehensive Survey Center, China Geological Survey,
    Changsha 410600, China; tangyuanyuan@mail.cgs.gov.cn
6   Guizhou Ecological Meteorology and Agrometeorology Center, Guiyang 550002, China;
    liaoyao10@mails.ucas.ac.cn
*   Correspondence: giantark@163.com; Tel.: +86-1393-3045-811

Abstract: This study investigates the dynamic changes in wheat canopy spectral characteristics across seven critical growth stages (Tillering, Pre-Jointing, Jointing, Post-Jointing, Booting, Flowering, and Ripening) using UAV-based multispectral remote sensing. By analyzing four key spectral bands—green (G), red (R), red-edge (RE), and near-infrared (NIR)—and their combinations, we identify spectral features that reflect changes in canopy activity, health, and structure. Results show that the green band is highly sensitive to chlorophyll activity and low canopy coverage during the Tillering stage, while the NIR band captures structural complexity and canopy density during the Jointing and Booting stages. The combination of G and NIR bands reveals increased canopy density and spectral concentration during the Booting stage, while the RE band effectively detects plant senescence and reduced spectral uniformity during the ripening stage. Time-series analysis of spectral data across growth stages improves the accuracy of growth stage identification, with dynamic spectral changes offering insights into growth inflection points. Spatially, the study demonstrates the potential for identifying field-level anomalies, such as water stress or disease, providing actionable data for targeted interventions. This comprehensive spatio-temporal monitoring framework improves crop management and offers a cost-effective, precise solution for disease prediction, yield forecasting, and resource optimization. The study paves the way for integrating UAV remote sensing into precision agriculture practices, with future research focusing on hyperspectral data integration to enhance monitoring models.

Keywords: UAV remote sensing; wheat growth stages; multispectral analysis; spatio-temporal monitoring; precision agriculture

1. Introduction

The development of precision agriculture has introduced new technical supports for crop growth monitoring, with UAV-based remote sensing emerging as an efficient data acquisition tool gaining increasing prominence in the agricultural sector [1,2]. As one of

the world's most important cereal crops, wheat production is directly tied to food security and agricultural economic efficiency [3]. The growth cycle of wheat is complex, spanning multiple critical stages from tillering to ripening, with significant variations in canopy characteristics, spectral reflectance properties, and growth status at each stage [3,4]. Traditional field-based observations can be time-consuming and labor-intensive and may not provide the same level of spatial and temporal resolution as UAV-based remote sensing. UAV remote sensing equipped with multispectral sensors enables efficient acquisition of canopy spectral information with high spatial resolution, enhancing crop growth monitoring from the tillering stage to the ripening stage [5–7].

Hyperspectral remote-sensing technologies have transformed agricultural monitoring by capturing detailed spectral data across narrow bands, offering insights into crop physiology and biochemistry [8]. Applications of this technology address key challenges such as yield prediction, stress detection, and resource optimization [2]. UAV-mounted hyperspectral cameras are particularly impactful due to their high spatial resolution and cost efficiency, complementing satellite-based and airborne platforms [9]. The visible spectrum (400–700 nm) supports chlorophyll monitoring, while RE (700–750 nm) and NIR (750–1400 nm) bands are crucial for assessing canopy health and structure [10]. Advanced indices like NDVI and CI, derived from these bands, enhance the sensitivity of monitoring models. Additionally, machine-learning algorithms like random forests and support vector machines improve the selection of optimal band combinations, boosting the accuracy of crop analysis [11].

Effective hyperspectral data analysis combines preprocessing, feature extraction, and advanced modeling techniques [12]. Preprocessing corrects distortions, while methods such as derivative spectroscopy and texture analysis reveal critical biophysical properties [13]. Machine-learning and deep-learning approaches, including convolutional and recurrent neural networks, enable precise analysis of growth dynamics and stress responses. These techniques facilitate applications like growth stage identification, early stress detection, and yield forecasting. However, challenges such as data redundancy, high costs, and a lack of standardized protocols hinder widespread adoption. Addressing these limitations requires innovative solutions for data management and algorithm development.

During wheat growth, the canopy characteristics and spectral responses undergo significant dynamic changes at each growth stage [14]. For example, the tillering stage is characterized by low canopy coverage, where the G band is highly sensitive to the inactive canopy [15]. During the jointing stage, canopy structural complexity significantly increases, with the NIR band responding strongly to these structural changes [16]. In the ripening stage, spectral reflectance uniformity declines, reflecting senescence and maturity. However, the application of UAV remote sensing to wheat growth stage monitoring still faces unresolved challenges, such as accurate growth stage classification, robust feature extraction, and the development of models that are both robust and transferable across different environmental conditions [17,18].

(1) How can key features of different wheat growth stages be accurately extracted from multispectral remote sensing data? The extraction of growth stage information relies on the selection of spectral bands and the quantification of critical features [11]. The G band reflectance captured the chlorophyll content of the plants, serving as an indicator of photosynthetic activity. The R band data facilitated the assessment of vegetation biomass and overall health, while the RE band, being highly sensitive to physiological changes, revealed subtle differences in plant growth. The NIR band reflectance was particularly valuable for evaluating wheat water content and biomass accumulation. Previous studies suggest that the G, R, RE, and NIR bands, along with their combinations, hold significant potential for reflecting plant health and canopy

structural changes [19]. However, there is a lack of systematic evaluation regarding the sensitivity and efficacy of these bands or combinations for different growth stages. Particularly, how to leverage multispectral data to distinguish stage-specific features amid the dynamic changes of the wheat growth cycle remains a scientific challenge.

(2) How can wheat growth be comprehensively monitored from a spatiotemporal perspective to support precision agricultural decision-making? The wheat growth cycle exhibits significant temporal and spatial heterogeneity. Temporally, dynamic changes in spectral characteristics across stages reveal canopy activity, health status, and stress conditions [20]. Spatially, the uniformity of canopy spectral reflectance, texture features, and localized anomalies within fields provide critical inputs for precision management [21]. Spectral data, texture information, and spatial distribution patterns contribute to precision management by offering insights into the wheat canopy's health, nutrient levels, and environmental conditions. These data are essential for making informed decisions regarding targeted fertilization, irrigation adjustments, and disease monitoring. However, existing research on integrating temporal monitoring with spatial distribution characteristics is insufficient, making it challenging to achieve systematic monitoring of the entire wheat growth cycle. This limitation not only constrains the application potential of remote sensing data in precision agriculture but also hinders a deeper understanding of the wheat growth process.

This study develops a comprehensive monitoring framework for the entire wheat growth cycle using UAV remote-sensing technology, addressing the two core scientific questions outlined above. Specifically, the research focuses on the following three aspects:

(1) We selected the G, R, RE, and NIR bands based on the spectral characteristics of wheat growth stages. Reflectance, entropy, variance, and other metrics were combined to quantify canopy health status and growth characteristics [22]. The sensitivity and efficacy of spectral band combinations in stage identification were thoroughly analyzed, providing foundational data for monitoring model development.

(2) We constructed dynamic feature models using multitemporal UAV remote-sensing data collected across seven growth stages for temporal monitoring and recognition. These models revealed spectral change trends and growth inflection points, providing insights into the spectral response patterns of wheat growth [23]. Temporal analysis clarified the dynamic characteristics of growth, offering a basis for yield prediction and stress diagnosis.

(3) By utilizing segmented mapping and spatial distribution models, the study analyzed the spectral uniformity and localized anomalies of the wheat canopy within fields [24]. The results of the distribution analysis informed precision farming strategies, including targeted fertilization, irrigation adjustments, and disease monitoring.

In response to the growing interest in deep-learning applications for hyperspectral and multispectral remote sensing, we have expanded the manuscript to include a comparison with recent deep-learning methods. Studies have shown the effectiveness of convolutional neural networks (CNNs), recurrent neural networks (RNNs), and other advanced deep-learning techniques in analyzing hyperspectral and multispectral data for crop monitoring. These methods have demonstrated promising results, particularly in feature extraction, classification, and prediction tasks. In contrast, our approach focuses on integrating temporal and spatial dynamics through UAV-based multispectral remote sensing, offering a comprehensive monitoring framework for wheat growth [25]. By comparing our methodology with these recent deep-learning models, we highlight the unique contributions and advantages of our model in precision agriculture applications, emphasizing its ability to track dynamic crop changes over time and space. The innovations of this study include:

The key innovation of this study lies in leveraging the temporal dimension to capture dynamic spectral changes across multiple critical growth stages, providing a more detailed and precise understanding of crop development compared to static analyses. The development of a spectral band combination analysis method based on multispectral remote sensing significantly enhances the accuracy of growth stage feature extraction [26,27]. The integration of temporal and spatial modeling establishes a comprehensive spatiotemporal monitoring framework for the entire wheat growth cycle. The linkage of monitoring results with precision agricultural management offers practical guidance for field management decisions [8]. This research provides valuable theoretical foundations and technical support for dynamic monitoring and comprehensive management of wheat growth, contributing to improved crop yields, resource efficiency, and sustainable agricultural practices.

Through these contributions, this research provides theoretical foundations and technical support for dynamic monitoring and comprehensive management of wheat growth while also serving as a reference for growth monitoring in other crops. Future directions emphasize integrating hyperspectral data with complementary remote-sensing technologies like LiDAR and thermal imaging to enhance multi-source analysis. Real-time monitoring platforms and open-access frameworks for data sharing and algorithm refinement are essential for fostering collaboration and scalability. Advances in machine learning tailored to hyperspectral applications will further optimize agricultural monitoring and resource management, driving innovation in precision agriculture.

UAV remote-sensing technology is crucial for agricultural monitoring and paves the way for future intelligent agricultural production [11,28,29]. The findings of this study not only advance the scientific development of wheat growth monitoring but also offer a technical roadmap and application paradigm for the innovation and dissemination of modern agricultural technologies. Future research should aim to integrate multisource remote-sensing data across larger areas to further explore the complex dynamics of crop growth, thereby enhancing the intelligence and efficiency of agricultural production systems.

2. Materials and Methods

2.1. The Study Area

The wheat experimental base of the Hebei Academy of Agriculture and Forestry Sciences (114°42′51.92″–114°43′29.61″ E, 37°56′36.36″–37°56′22.87″ N) was selected as the study area (Figure 1). Located at an average altitude of 55 m above sea level, the base covers approximately 7.2 hectares (0.072 square kilometers). As one of China's premier institutions for wheat research, the base leverages the unique natural resources and agricultural advantages of Hebei Province to establish a comprehensive research system encompassing wheat breeding, cultivation techniques, and pest and disease management [30,31] within a semi-humid and semi-arid region characterized by a warm temperate continental monsoon climate. The average annual temperature is 13.3 °C, with summer peaks averaging 26.9 °C and winter lows averaging −2.4 °C. Annual precipitation averages 534.6 mm, mainly concentrated in July and August, resulting in uneven seasonal distribution. The region features light and medium loam soils, suitable for agriculture but with some areas exhibiting lower nutrient content. Agricultural management practices, including modern park development and soil pollution control, help ensure agricultural product quality. These environmental and agricultural factors significantly impact wheat growth and were considered in the experimental design.

The base focuses on the growth mechanisms, quality improvement, and stress resistance of wheat, aiming to drive sustainable development and technological innovation in the wheat industry [32]. Within the base, the research team conducts large-scale ex-

periments and data collection to systematically analyze wheat growth patterns and yield performance under various environmental conditions [33].
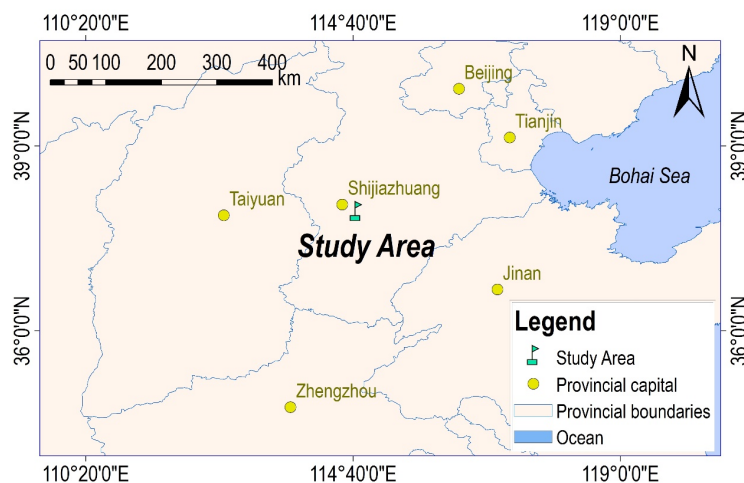
Figure 1. Location of wheat growing area in experimental field. The study area is located 20 km southeast of Shijiazhuang, the capital of Hebei Province.

This research platform provides a solid foundation for understanding the dynamic growth processes of wheat, offering critical insights into yield optimization, disease resistance, and adaptive management under changing agricultural environments [34]. Through interdisciplinary efforts and continuous innovation, the Hebei wheat experimental base contributes to advancing China's wheat production efficiency and sustainability.

2.2. Data Sources and Processing

Using the DJI Phantom 4 UAV (DJI Innovations, Shenzhen, Guangdong, China) equipped with six 1/2.9-inch CMOS sensors, including one color sensor for visible light imaging and five monochrome sensors for multispectral imaging, multispectral data of wheat at various growth stages were collected [35]. The multispectral sensors covered four key spectral bands: the G band with a central wavelength of 560 nm, the R band at 650 nm, the RE band at 730 nm, and the NIR band at 840 nm [36]. We selected these bands to capture the spectral responses of crops, providing critical information on plant health, nutrient levels, and water status. Specifically, the RE and NIR bands demonstrated significant correlations with wheat growth status and biomass, offering essential indicators for crop monitoring [37]. We calibrated the reflectance data before and after each flight to ensure the accuracy of the spectral measurements. The panel was placed in representative locations within the study area, and preliminary measurements were made to adjust for any atmospheric conditions or sensor discrepancies. This process was repeated after each flight to ensure consistent data quality throughout the experiment.

During the experiments, the UAV operated at a flight altitude of 20 m, balancing spatial resolution and coverage. The spatial resolution achieved by Phantom 4 was 0.01 m, ensuring image clarity and detailed richness. This high-resolution imagery provided a reliable foundation for subsequent data analysis, enabling more accurate identification of wheat growth characteristics and potential issues [1].

To obtain accurate canopy reflectance values, the UAV data underwent a series of processing steps, including radiometric calibration, atmospheric correction, and regional cropping. Initially, metadata were extracted from the raw UAV imagery and parsed to identify key parameters such as central wavelengths, full width at half maximum (FWHM), calibration coefficients, and coordinate information for each spectral band. This information was then processed to ensure accurate calibration of the reflectance data, with each
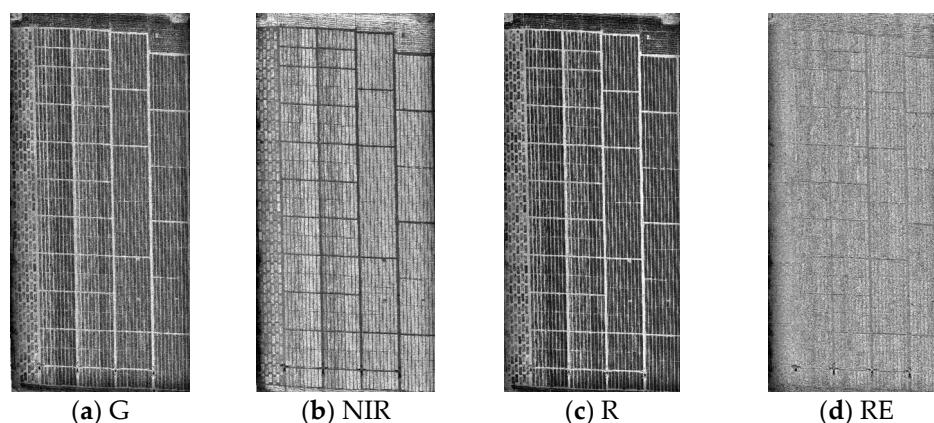
parameter being cross-referenced and validated for consistency across all data points [38]. The gray values were then converted into absolute radiance values, translating digital numbers into physically meaningful apparent radiance values, thereby determining the radiance at the sensor aperture [39]. Ground calibration data were collected synchronously to perform atmospheric corrections, aiming to eliminate radiance errors caused by atmospheric absorption and scattering and to derive true reflectance values for wheat. Finally, distribution maps of wheat were imported and extraneous data were cropped, generating multispectral images of wheat canopy reflectance [40]. The calibration method based on the built-in solar sensor of the drone was not applied in this study. On the contrary, we rely on a relative calibration method based on ground black and white cloth. These images provided essential baseline data for monitoring growth status and ecological assessments, ensuring the comparability of multispectral data collected across different periods. The UAV images were processed using Photoscan software (3.11.0, Python Software Foundation, Wilmington, DE, USA) to generate multispectral orthomosaics. The photogrammetric tools and algorithms in Photoscan ensured high geometric accuracy during the image-stitching process. For reflectance calibration, we used Python-based scripts to correct the raw reflectance values and account for atmospheric effects. Python-based scripts were used for reflectance calibration, utilizing libraries such as numpy and scipy for data manipulation and pyproj for coordinate transformations. For atmospheric correction, tools like Py6S or similar atmospheric correction libraries were employed to account for atmospheric scattering and absorption effects, ensuring the accuracy of the reflectance values. During the post-processing phase, we applied segmentation methods to eliminate the influence of ground reflectance and other potential sources of background noise, such as soil and shadows. This process ensured that the reflectance data were attributable solely to the vegetation cover, providing accurate measurements of plant health and growth.

In this study, UAV multispectral data were collected at seven time points between March and June, corresponding to key stages of the wheat growth cycle, including the Tillering, Jointing, Booting, Flowering, and Ripening stages [41]. This data acquisition process aimed to comprehensively monitor the growth status and health of wheat at various stages, facilitating a deeper analysis of growth patterns and influencing factors. At each growth stage, UAV multispectral imaging technology was used to acquire high-resolution hyperspectral reflectance data of the wheat canopy. Tillering Stage (March to early April): Wheat begins tillering, forming multiple tillers, which enhance root systems and stems. Jointing Stage (early April to late April): Stems elongate, and internodes grow, laying the foundation for subsequent ear differentiation. Booting Stage (late April to mid-May): Ears form and gradually mature. Flowering Stage (mid-May to late May): Ears begin flowering and pollination occurs. Ripening Stage (late May to mid-June): Grains mature, moisture content decreases, and plants prepare for harvest. Additional data collection during the Jointing Stage included Pre-Jointing and Post-Jointing stages to capture the dynamic changes in wheat growth comprehensively. We selected these time points to reflect key transitions and growth dynamics throughout the wheat lifecycle [20] (Table 1).

These data provided critical information for analyzing the growth characteristics of wheat at this specific time point [42]. The true-color image offered an overview of the wheat's appearance and general health status. By integrating and analyzing these spectral bands, we gained a comprehensive understanding of the growth dynamics of wheat at this stage (Figure 2). This multifaceted approach not only highlights the physiological and structural characteristics of the crop but also supports precise monitoring of its developmental status.

Table 1. Overview of wheat growth stages and collection dates. This table displays the collection dates of drone multispectral data for wheat at different growth stages from March to May 2024, facilitating the subsequent analysis of wheat growth dynamics and health status.

Serial Number	Date	Different Growth Stages of Wheat						
		Tillering Stage	Pre-Jointing Stage	Jointing Stage	Post-Jointing Stage	Booting Stage	Flowering Stage	Ripening Stage
1	11 March 2024	√						
2	1 April 2024		√					
3	23 April 2024			√				
4	30 April 2024				√			
5	9 May 2024					√		
6	21 May 2024						√	
7	28 May 2024							√

(a) G   **(b)** NIR   **(c)** R   **(d)** RE

Figure 2. Multispectral bands and true color images of wheat growth characteristics. This set of images displays the reflectance characteristics of wheat on 11 March 2024, for the G, R, RE, and NIR bands. By comparing the images from each band, we can clearly observe the growth status, health levels, and physiological characteristics of wheat at this growth stage, providing intuitive visual support for further analysis.

2.3. Spectral Algorithm

In response to the suggestion that the operation between spectral bands should involve more complex combinations similar to vegetation indices, we have elaborated on the basis and theoretical underpinnings of these combinations in the spectral algorithm. These combinations are derived from biophysical and biochemical principles of crop physiology, specifically focusing on chlorophyll absorption, canopy structure, and water content dynamics, which are critical for understanding crop growth and health.

The G band is highly sensitive to chlorophyll absorption, a key indicator of plant photosynthesis, and is often used in calculating vegetation indices such as the Normalized Difference Vegetation Index (NDVI). The R band, being another key indicator of chlorophyll absorption, complements the G band, as its reflectance is inversely related to chlorophyll content. The NIR band, which reflects the canopy's structural properties and water content, plays a significant role in understanding plant health, particularly in detecting variations in leaf area and water stress. By combining these bands, we can enhance the detection of complex physiological conditions, such as leaf density, canopy health, and water content. For example, combinations of the G and NIR bands are particularly effective for monitoring canopy health and leaf density, as the NIR band is sensitive to plant structure and the G band responds to photosynthetic activity. Similarly, combining the RE and NIR bands has

proven valuable in assessing plant health during stages of active growth or senescence, as the RE band is sensitive to physiological changes in the plant, such as chlorophyll content and leaf maturity.

Additionally, we have incorporated references to previous studies that validate the use of these spectral combinations in remote-sensing applications. Vegetation indices such as NDVI and the Enhanced Vegetation Index (EVI), which utilize the G, R, and NIR bands, have been widely used to monitor plant health, water stress, and nitrogen content. These indices have been shown to effectively capture variations in canopy health and biomass, further supporting the use of multi-band combinations in our spectral algorithm. This integration of biophysical principles and proven remote-sensing techniques enhances the algorithm's ability to track dynamic crop characteristics and monitor growth stages more accurately. It allows for a more precise and comprehensive assessment of crop health, stress, and physiological development across different stages of growth.

For remote-sensing images containing four spectral bands, various image feature values can be calculated through different band combinations [39]. Specifically, the combinations can be categorized into single-band, two-band, three-band, and four-band combinations, resulting in a total of 15 possible combinations (Table 2).

(1) Single-band combinations: Selecting one band from the four available bands yields $C(4,1) = 4$ combinations. Single-band combinations are commonly used to extract basic features such as brightness and reflectance. They are particularly effective in analyzing the behavior of specific bands under particular conditions, such as using the blue band for water monitoring because of its high absorption by water, or the NIR band for vegetation analysis because of its strong sensitivity to plant chlorophyll. Single-band analysis is often employed as an initial screening tool to identify anomalies.

(2) Two-band combinations: Selecting two bands from the four yields $C(4,2) = 6$ combinations. Two-band combinations are useful for analyzing relative relationships between bands. For example, ratio analysis can highlight specific features of certain land-cover types. These combinations are widely used for calculating ratio-based indices, such as vegetation coverage monitoring. They are effective in distinguishing different land-cover types and are particularly helpful for analyzing mixed pixels, offering insights into the contributions of various land covers within a single pixel.

(3) Three-band combinations: Selecting three bands from the four results in $C(4,3) = 4$ combinations. This approach is commonly used to compute specific composite indices. Three-band combinations are suitable for deriving more complex indices and extracting detailed features of land covers. By leveraging texture features from three bands, these combinations enhance the understanding of land cover structures and provide a deeper interpretation of surface properties.

(4) Four-band combinations: Utilizing all four bands yields $C(4,4) = 1$ combination. Four-band combinations provide comprehensive information, making them ideal for analyzing complex scenarios. These combinations are particularly suited for applications requiring multidimensional data, offering richer information to support fine-grained classification and analysis. Four-band combinations enable an integrated approach to understanding the relationships among spectral features, facilitating holistic and detailed analyses.

These band combinations and their respective feature extraction capabilities play a crucial role in advancing the understanding and interpretation of complex remote-sensing datasets, supporting diverse applications from anomaly detection to precise land-cover classification [19,43].

Table 2. Different band combinations and calculation formulas for remote-sensing images. The table displays various transformation methods for single band, dual band, triple band, and quadruple band, facilitating analysis and extraction of image features.

Serial Number	Transformation Method	Process Formulas
1	Single-band G	$X_i = R_G$
2	Single-band NIR	$X_i = R_{NIR}$
3	Single-band R	$X_i = R_R$
4	Single-band RE	$X_i = R_{RE}$
5	Dual-band G-NIR	$X_i = R_G / R_{NIR}$
6	Dual-band G-R	$X_i = R_G / R_R$
7	Dual-band G-RE	$X_i = R_G / R_{RE}$
8	Dual-band NIR-R	$X_i = R_{NIR} / R_R$
9	Dual-band NIR-RE	$X_i = R_{NIR} / R_{RE}$
10	Dual-band R-RE	$X_i = R_R / R_{RE}$
11	Triple-band G-NIR-R	$X_i = R_G + R_{NIR} + R_R$
12	Triple-band G-NIR-RE	$X_i = R_G + R_{NIR} + R_{RE}$
13	Triple-band G-R-RE	$X_i = R_G + R_R + R_{RE}$
14	Triple-band NIR-R-RE	$X_i = R_{NIR} + R_R + R_{RE}$
15	Quadruple-band G-NIR-R-RE	$X_i = R_G + R_{NIR} + R_R + R_{RE}$

Note: X_i is the processed spectral reflectivity; R_i the reflectivity corresponding to the wavelength.

2.4. Feature Extraction Algorithm

When extracting UAV imagery of wheat at different growth stages, it is essential to design a series of feature extraction algorithms to accurately identify and analyze the growth status and health levels of the crop [2,44]. These algorithms target different growth stages, focusing on extracting key features such as color, texture, and shape, to better understand the growth dynamics of wheat. This study selected 15 indicators (Table 3) that comprehensively reflect the image characteristics during the wheat growth process from various perspectives. These indicators enable an in-depth analysis of growth status, health levels, and growth patterns, providing valuable data support for precision agriculture. By employing a combination of image processing techniques, including statistical analysis, machine learning, and deep learning, the accuracy and efficiency of feature extraction can be significantly enhanced, laying a solid data foundation for subsequent growth monitoring and management [45].

The variables included in Table 3 were selected based on their established relevance in remote sensing and image analysis, particularly for crop monitoring. These variables, such as entropy, contrast, and texture variance, are critical for capturing key aspects of canopy health, structural complexity, and dynamic changes that occur across different growth stages of crops. In remote-sensing applications, entropy measures the complexity of pixel-value distributions within an image, providing insights into the structural heterogeneity of the canopy. Higher entropy values typically reflect more complex canopy structures, which are indicative of dynamic changes in plant health and growth. Contrast, on the other hand, quantifies the difference in pixel intensities between adjacent areas in the image. This metric is valuable for detecting variations in canopy texture, which are associated with differences in plant health, leaf area, and vegetation stress. Texture variance measures the variability in pixel values across the image, reflecting the degree of canopy complexity. Variance is sensitive to changes in canopy architecture and is particularly useful for detecting early signs of stress, such as nutrient deficiencies or disease.

Table 3. Statistical measures and their implications for image analysis. This table summarizes key statistical measures used in image analysis, highlighting their formulas, meanings, and applications for evaluating various aspects of image quality and texture.

Serial Number	Calculate Indicators	Process Formulas	Meaning and Purpose
1	Mean	$\mu = \frac{1}{N} \sum_{i=1}^{N} B_i$	The average value of pixel values reflects the overall brightness of the image. Used to evaluate the brightness level of images.
2	Variance	$\sigma^2 = \frac{1}{N} \sum_{i=1}^{N} (B_i - \mu)^2$	The degree of dispersion of pixel values reflects the contrast of an image. Used for analyzing the brightness distribution of images.
3	Standard Deviation	$\sigma^2 = \sqrt{\sigma^2}$	The square root of variance represents the degree of fluctuation in pixel values. To evaluate the stability of image brightness.
4	Entropy	$H = -\sum_{i=1}^{N} p(B_i) log_2 p(B_i)$	The uncertainty of pixel value distribution, the higher the entropy value, the more complex the image. Used for image complexity and texture analysis.
5	Skewness	$S = \frac{1}{N} \sum_{i=1}^{N} \left(\frac{B_i - \mu}{\sigma} \right)^3$	The symmetry of pixel value distribution, with positive skewness indicating right skewness and negative skewness indicating left skewness. Used for analyzing the deviation of brightness distribution.
6	Kurtosis	$K = \frac{1}{N} \sum_{i=1}^{N} \left(\frac{B_i - \mu}{\sigma} \right)^4 - 3$	The sharpness of pixel value distribution, with high peak indicating the data set. Used to analyze the concentration of brightness distribution.
7	Brightness Range	$R_g = B_{max} - B_{min}$	The difference in pixel values in an image represents the dynamic range. To evaluate the contrast and dynamic range of images.
8	Root Mean Square	$RMS = \sqrt{\frac{1}{N} \sum_{i=1}^{N} B_i^2}$	The root mean square of pixel values reflects the brightness intensity of an image. To measure the overall intensity of image brightness.
9	Brightness Concentration	$R_c = \sum_i p(B_i) \cdot B_i$	The weighted average of pixel values represents the degree of concentration of brightness. Used for analyzing image brightness distribution.
10	Contrast	$R_{tm} = \sum_{i,j} (i-j)^2 P(i,j)$	The average value of the texture matrix reflects the texture features. To evaluate the texture features of images.
11	Texture Variance	$R_{tv} = \frac{1}{N} \sum_{i,j} (P(i,j) - R_{tm})^2$	The variance of the texture mean represents the degree of texture dispersion. To evaluate the consistency of image texture.
12	Frequency Entropy	$H_f = -\sum_i f_i log_2 f_i$	The entropy value of the frequency distribution of pixel values reflects the diversity of brightness. To evaluate the diversity of image brightness distribution.

Table 3. *Cont.*

Serial Number	Calculate Indicators	Process Formulas	Meaning and Purpose
13	Texture Entropy	$H_t = -\sum_{i,j} P(i,j) log_2 P(i,j)$	The entropy value of the texture matrix represents the complexity of the texture. To evaluate the texture complexity of images.
14	Energy	$E = \sum_{i,j} P(i,j)^2$	It is the total energy calculated through the feature matrix in texture feature extraction. To evaluate the richness of information in the image.
15	Brightness Correlation	$C = \sum_{i,j} B_i \cdot B_j / N$	An indicator that describes the relationship between the brightness values of different pixels in an image. To evaluate the consistency and similarity of image brightness distribution.

Note: μ is the mean value of pixels; N is the total number of pixels; i is the pixel number; B_i is the i-th pixel value; σ^2 is the variance; H is the entropy; $p(B_i)$ is the probability of the i-th pixel value; S is the skewness; K is the kurtosis; R_g is the brightness range; B_{max} and B_{min} are the maximum and minimum pixel values, respectively; RMS is the root mean square; R_c is the brightness centration; R_{tm} is the contrast; $P(i,j)$ is the pixel values of texture matrix; R_{tv} is the texture variance; H_f is the frequency entropy; f_i is the probability of the i-th pixel value; H_t is the texture entropy; E is the energy value; C is the Brightness Correlation; B_i and B_j are the pixels to be calculated.

These selected variables play an essential role in accurately assessing crop health, identifying stress conditions, and monitoring growth transitions. By leveraging these metrics, the analysis provides a comprehensive understanding of canopy dynamics, enabling more precise monitoring of crop development. The inclusion of these variables is supported by extensive research in the field, where similar metrics have been demonstrated to improve the accuracy of crop monitoring and yield prediction models. Relevant studies have shown that these variables are particularly effective in distinguishing different growth stages and detecting anomalies related to plant health and environmental factors. By incorporating these well-established metrics into the spectral algorithm, this study enhances the ability to capture subtle changes in crop physiology and offers a more robust framework for monitoring crop health throughout the growing season. The updated manuscript further clarifies the rationale for selecting these variables, and references to relevant studies have been included to substantiate their use in remote-sensing and crop monitoring applications.

By extracting features from UAV imagery collected during seven distinct growth stages, we can capture the dynamic growth patterns of wheat [39]. The analysis of these features facilitates the identification of differences between growth stages, predicts wheat growth trends, and informs the development of appropriate management strategies. Using a data-driven approach allows for more effective crop monitoring, optimized resource allocation, and improvements in both wheat yield and quality [36]. These efforts collectively contribute to advancing the application of precision agriculture, ensuring sustainable and efficient crop production.

2.5. Data Post-Processing Methods

In multi-temporal remote-sensing monitoring, the spectral reflectance characteristics and spatial texture information of wheat at different growth stages vary dynamically throughout the growth process [12]. These features can reflect critical growth parameters such as leaf area index (LAI), vegetation coverage, and health status. However, due to the differing calculation methods and physical meanings of remote-sensing features, there are significant differences in their dimensions and value ranges. For instance, brightness may range from 0 to 65,535, whereas contrast and entropy are typically represented as

small decimal values. Directly using these feature data for modeling and analysis may lead to certain features being either excessively amplified or completely ignored in the model, thereby reducing the accuracy and scientific validity of the analysis results [46].

The primary purpose of normalization is to map different feature values into a unified range (typically [0, 1]) while preserving the trends of feature variations. The calculation formula is:

$$x' = \frac{x - \min(x)}{\max(x) - \min(x)} \tag{1}$$

In the formula, x represents the original feature value, $\min(x)$ is the minimum value of the feature column, $\max(x)$ is the maximum value of the feature column, and x' is the normalized feature value. This processing method eliminates the interference caused by differences in dimensions, ensuring that all features have equal importance in subsequent analyses [23]. Additionally, normalization improves the training efficiency and convergence speed of models, thereby enhancing the predictive performance of wheat growth models.

By normalizing various features extracted from UAV remote-sensing data, a reliable foundation is provided for quantitative comparisons of wheat growth conditions across different growth stages [47]. The normalized feature data intuitively reflect the temporal variation patterns of wheat growth, aiding in the identification of key growth characteristics at different stages and providing a scientific basis for precision agricultural management. Furthermore, this data processing approach improves the generalizability of analyses, enabling models to adapt to data from different regions and wheat varieties. This adaptability supports large-scale remote-sensing monitoring and crop production decision-making [7].

Wheat growth models built using normalized feature data not only provide higher accuracy for monitoring growth but also offer critical data support for yield prediction, disaster warning, and precision agricultural management [47]. This ensures that remote-sensing applications can effectively support sustainable and efficient agricultural practices at multiple scales.

2.6. Statistical Analysis

In this study, we performed all statistical analyses using Python (version 3.12.3), utilizing the scipy, statsmodels, and numpy libraries for conducting the necessary tests. Due to the research objectives and the nature of the data, we employed *t*-tests to evaluate the relationships between variables and test our hypotheses. These methods were selected based on their ability to analyze the impact of independent variables on a dependent variable, which directly aligns with the goals of our study.

For the assumptions underlying the statistical tests, we performed the following diagnostic checks: we assessed the normality of the data using the Shapiro–Wilk test and visually examined histogram plots. The assumption of homogeneity of variance was tested using Levene's test, ensuring that the variability between groups was consistent. In cases of regression analysis, we examined residual plots to check for linearity and homoscedasticity. The significance level was set at $p < 0.05$ for all tests, in accordance with standard practice in our field. All analyses were performed with careful consideration of the assumptions and methods selected, ensuring the robustness and validity of our findings.

3. Results

3.1. Remote-Sensing Feature Calculation Results Under 15 Band Combinations

We constructed heatmaps and boxplots to analyze the feature distribution and variation patterns of UAV remote-sensing data. Heatmaps visually present the dynamic trends of various features over time during the wheat growth process through variations in color intensity, reflecting the spatiotemporal changes in spectral and texture features across

different growth stages [17]. This visualization approach allows for the rapid identification of significant feature value change intervals, highlighting key features that influence the growth process. Additionally, boxplots describe the distribution range, central tendency, and outliers of each feature, illustrating the stability and variability of features at different time intervals [15].

Different band combinations show significant differences and complementarities in monitoring the dynamic growth of wheat, providing critical insights for comprehensively evaluating canopy characteristics and health status [7,48] (Figure 3). The left panel of Figure 3 shows the normalized calculation results of different feature values. The purpose of this visualization is to standardize the feature values, eliminating the impact of varying scales or units between different variables. By normalizing the values, it becomes easier to compare the relative changes in each feature, regardless of their original magnitudes. This approach allows for a clearer understanding of how each feature behaves over time and provides a uniform basis for comparing different spectral characteristics. Normalization ensures that the data's trends and patterns are not skewed by differences in their value ranges, making the analysis more reliable and interpretable. The right panel, on the other hand, displays the normalized calculation results of different feature values across the seven growth stages (1–7). This visualization is crucial because it illustrates how the spectral characteristics of the crop evolve at each specific growth stage. By presenting the normalized feature values for each growth stage, this panel provides insights into the temporal dynamics of canopy health, leaf area, and stress levels. The comparison across growth stages allows for a better understanding of the crop's physiological changes throughout its life cycle, helping to pinpoint critical periods for intervention (e.g., fertilization, irrigation) and stress monitoring. Overall, this approach enhances the ability to track crop growth with higher precision and supports targeted agricultural management strategies.

The G band is most sensitive to vegetation activity during the Jointing and Booting stages, characterized by high brightness values (mean reaching 0.80) and low texture complexity (variance around 0.05), making it suitable for reflecting the spectral characteristics of vigorous growth stages. The NIR band excels in assessing water stress and canopy health, with entropy values reaching 1.2 under disease stress, indicating changes in canopy texture complexity. The R band primarily reflects the spectral stability of the canopy during the ripening stage, with root-mean-square values dropping to 0.5 in the late growth stages, while kurtosis and contrast reveal the stability of spectral reflectance. The RE band strongly indicates nitrogen absorption and health monitoring, with median brightness reaching 0.85 during the Jointing stage.

Band combinations further enhance sensitivity and stability in detecting wheat growth characteristics [34,43]. The G + NIR combination achieves a mean value of 0.85 during the Jointing stage, making it suitable for reflecting canopy density and activity. The G + R combination shows increasing contrast over time, reflecting the dynamic changes in canopy structure during the growth stages. The G + RE combination responds strongly to spectral variations in wheat, while the NIR + R combination is better suited for health monitoring, with skewness peaking at 0.5 during the Grain Filling stage. Three-band combinations, such as G + NIR + R and G + NIR + RE, further enhance the dynamic response to vigorous growth and decline stages. Meanwhile, the four-band combination (G + NIR + R + RE) offers the most comprehensive assessment of texture and spectral changes across the entire growth cycle. These findings demonstrate that single bands are suitable for monitoring specific stages, while multi-band combinations enable full-cycle monitoring of wheat growth characteristics [19]. This provides scientific support for precision agricultural management, disease monitoring, and yield prediction.
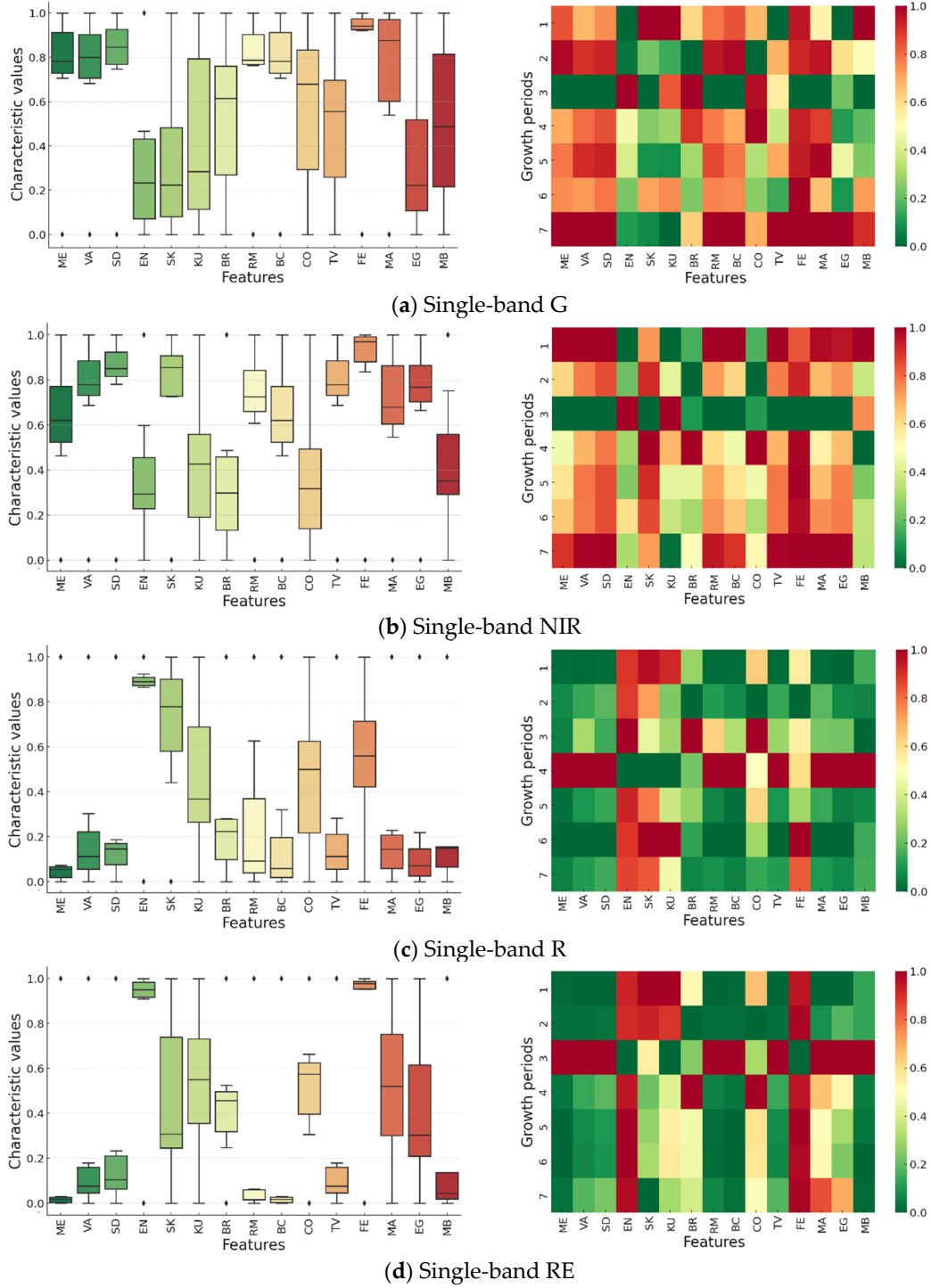
(**a**) Single-band G
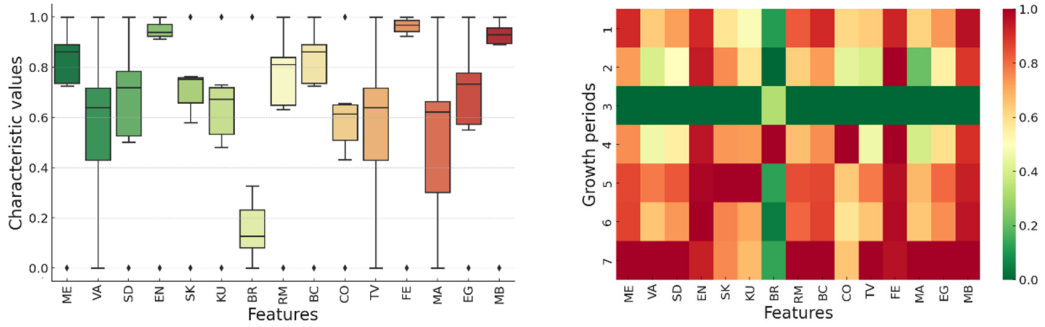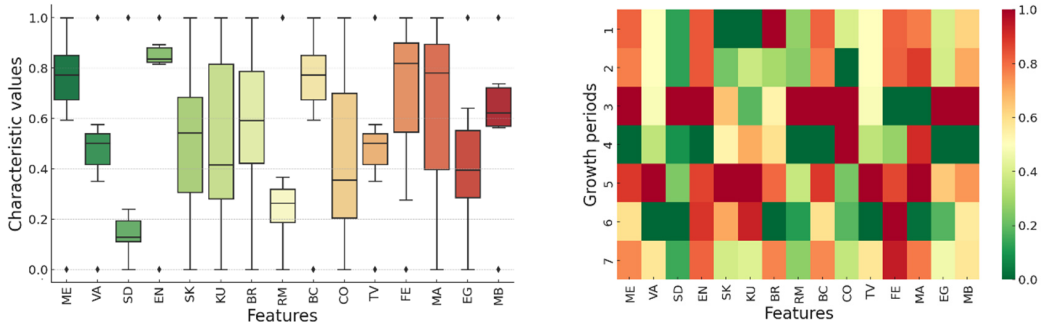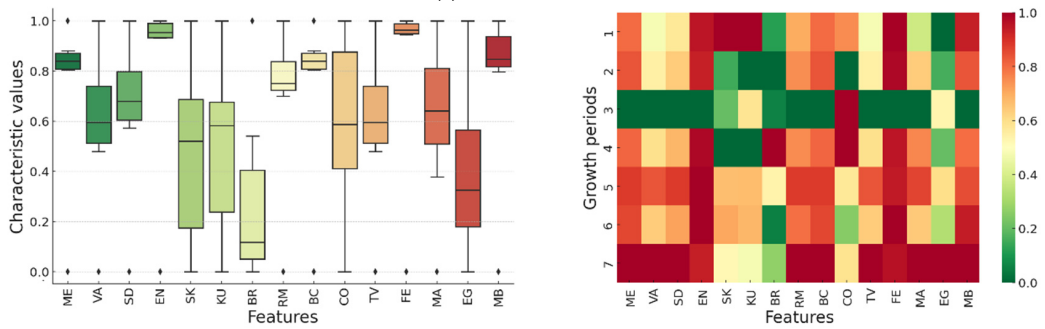

(**b**) Single-band NIR

(**c**) Single-band R

(**d**) Single-band RE

Figure 3. *Cont.*

(**e**) Dual-band G-NIR

(**f**) Dual-band G-R

(**g**) Dual-band G-RE

(**h**) Dual-band NIR-R

(**i**) Dual-band NIR-RE

Figure 3. *Cont.*

(**j**) Dual-band R-RE

(**k**) Triple-band G-NIR-R

(**l**) Triple-band G-NIR-RE

(**m**) Triple-band G-R-RE

(**n**) Triple-band NIR-R-RE

Figure 3. *Cont.*

(**o**) Quadruple-band G-NIR-R-RE
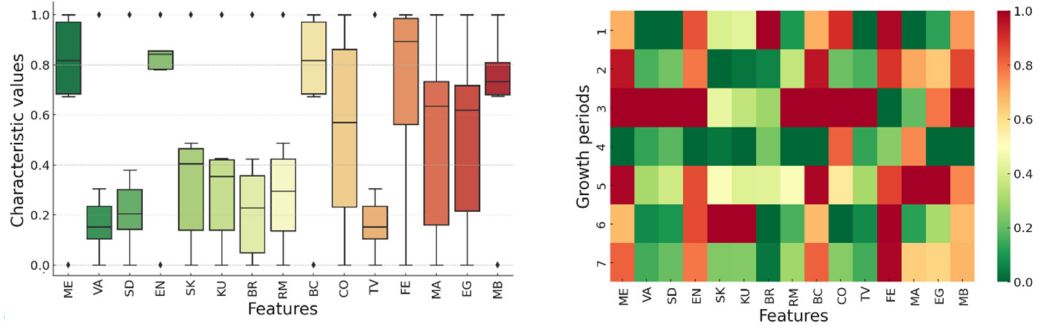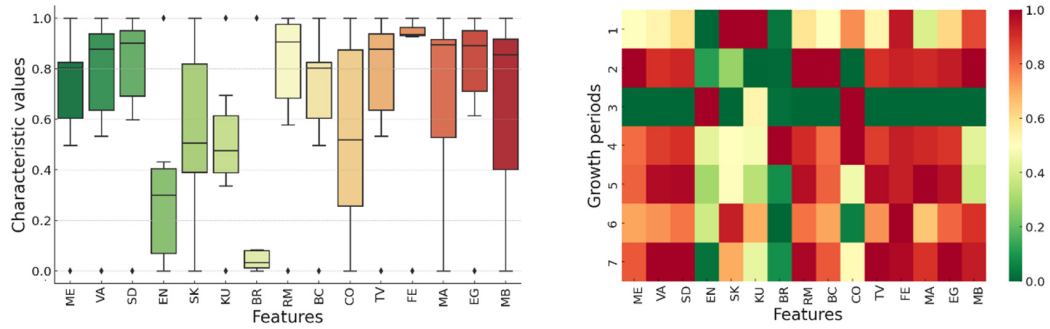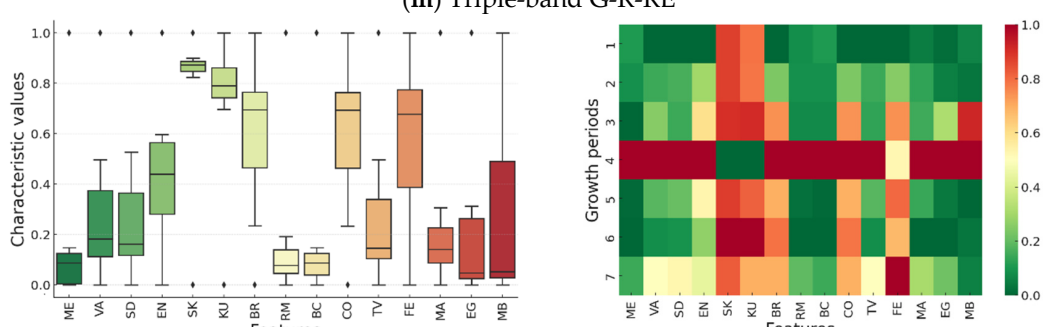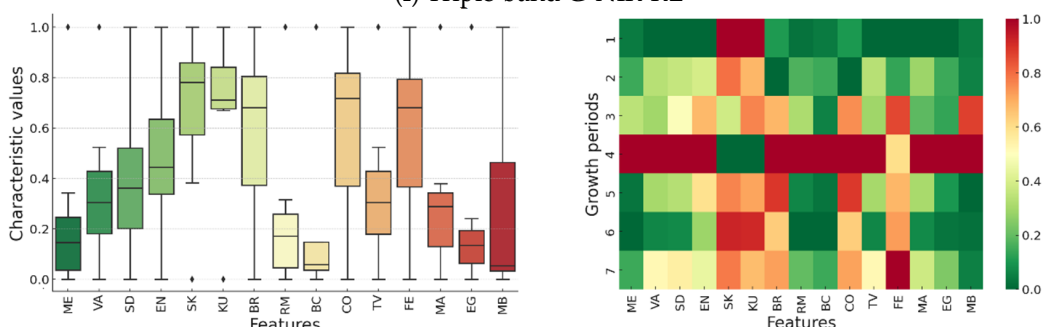
Figure 3. Multidimensional visualization analysis of wheat growth dynamics using UAV remote sensing. (**a**) G band: Reflects high vegetation activity, suitable for monitoring canopy changes. (**b**) NIR: Indicates healthy growth and water stress conditions. (**c*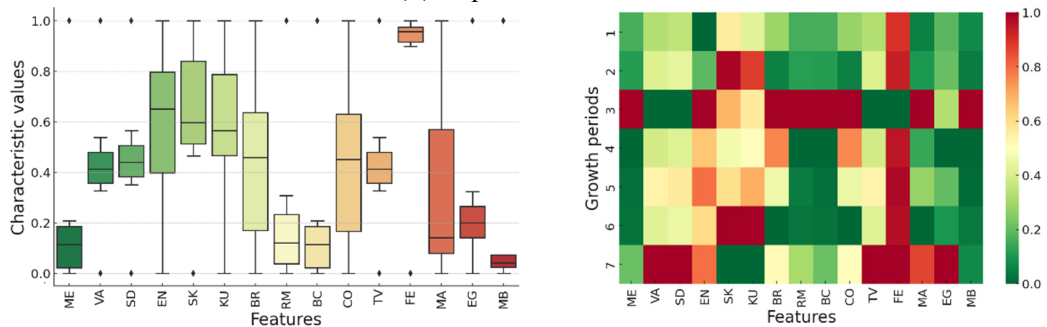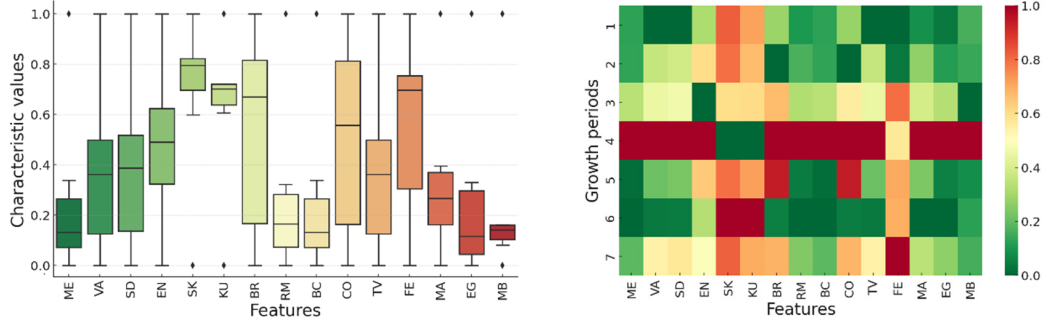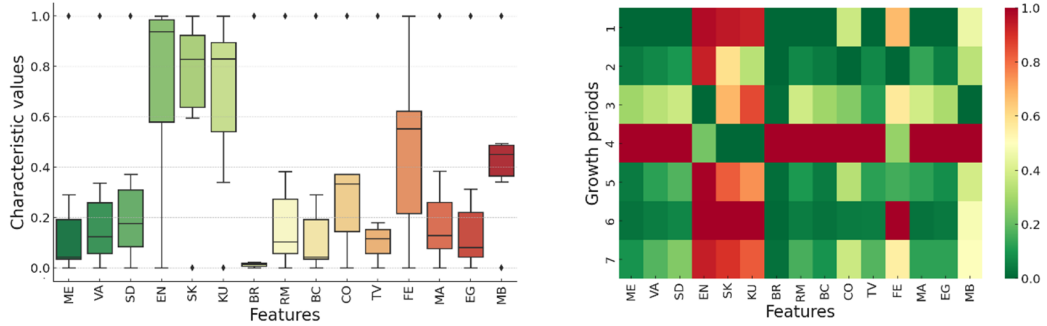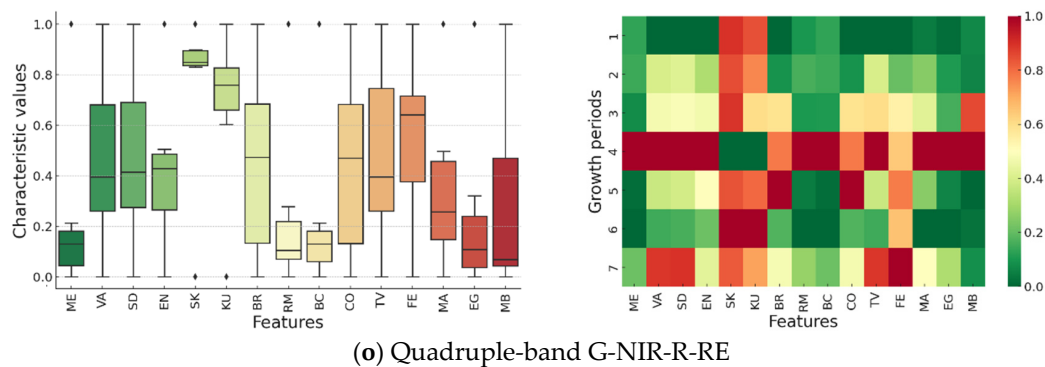*) R: Represents stability during the maturity stage. (**d**) RE band: Suitable for monitoring nitrogen uptake and plant health. (**e**) G + NIR: Reflects chlorophyll content and canopy density. (**f**) G + R: Demonstrates dynamic changes in canopy structure. (**g**) G + RE: Suitable for spectral dynamics monitoring. (**h**) NIR + R: Reflects disease stress and healthy areas. (**i**) NIR + RE: Indicates water stress and healthy conditions. (**j**) R + RE: Reflects maturity characteristics. (**k**) G + NIR + R: Useful for monitoring disease stress. (**l**) G + NIR + RE: Tracks spectral changes across growth stages. (**m**) G + R + RE: Monitors texture changes in the canopy. (**n**) NIR + R + RE: Suitable for disease-stress monitoring. (**o**) G + NIR + R + RE: Ideal for dynamic analysis across the growth cycle.

3.2. Remote-Sensing Analysis of Seven Growth Stages of Wheat

Using UAV-based remote-sensing technology, the seven critical growth stages of wheat can be precisely monitored to assess vegetation coverage, canopy structure, health status, and growth dynamics [1]. The analysis of these time-series data not only reveals the physiological characteristics of each stage but also provides scientific guidance for disease warning, precision fertilization, and yield prediction [8]. Feature extraction across these growth stages facilitates optimized crop management, enhances agricultural productivity, and promotes the application of remote-sensing technology in precision agriculture, thereby offering robust data support for sustainable agricultural development by optimizing resource use, improving crop yield predictions, enabling early detection of pests and diseases, and supporting more precise decision-making for irrigation, fertilization, and pest control (Figure 4).

Figure 4 illustrates the spectral characteristics of wheat across different growth stages, represented through a radar chart. Each segment of the radar chart corresponds to a specific growth stage (1–7), with the various axes reflecting different spectral features or variables, such as the reflectance values from different spectral bands (G, R, RE, NIR). The chart displays how these features evolve over time as the crop progresses through its growth stages, providing a clear visual representation of changes in the spectral properties of wheat at each critical growth phase.

The purpose of Figure 4 is to facilitate the comparison of spectral changes at different growth stages, highlighting key shifts in crop characteristics like canopy health, leaf area, and stress levels. By using a radar chart, the figure effectively communicates the multidimensional nature of crop growth dynamics and helps identify important growth transitions. This enables a better understanding of how the crop's spectral features evolve, which is crucial for precision agriculture and supports decisions related to intervention timing and stress detection. In Figure 4, the highlighted line emphasizes the key trends or significant variations in spectral characteristics at each growth stage. This line allows readers to easily track the most notable shifts in the crop's spectral features, such as changes in canopy health, chlorophyll content, or plant stress levels. It also helps identify critical

growth stages where substantial transitions occur, facilitating a more focused analysis of the crop's development and making it easier to correlate spectral data with physiological changes for informed crop management decisions.
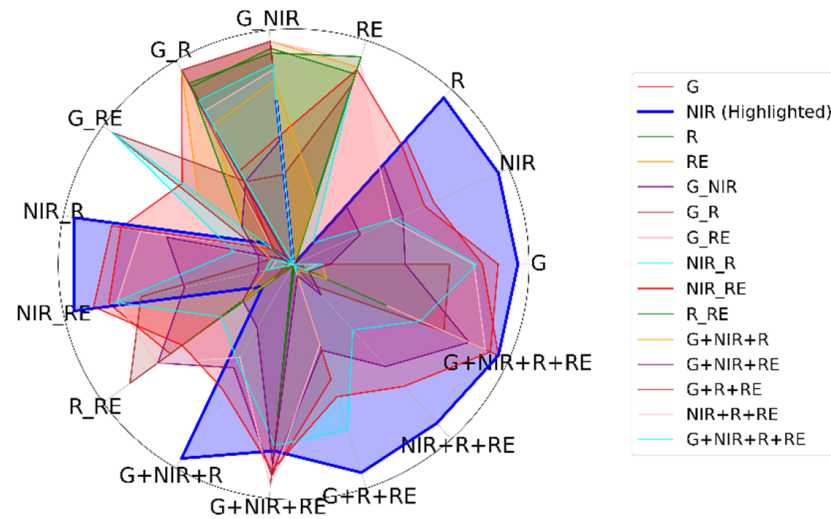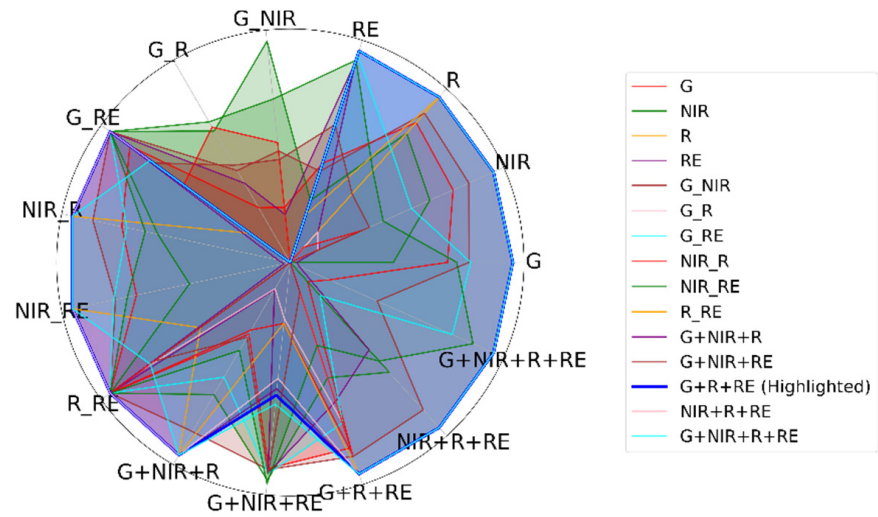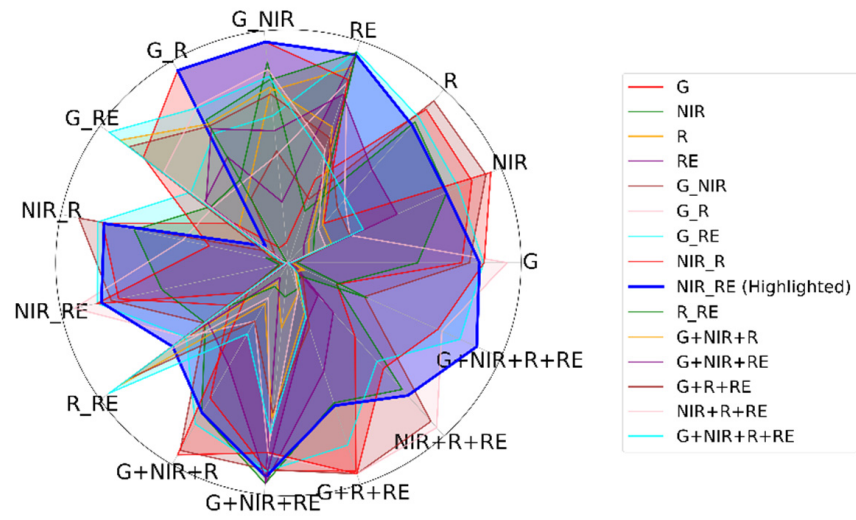

(**a**) Tillering Stage
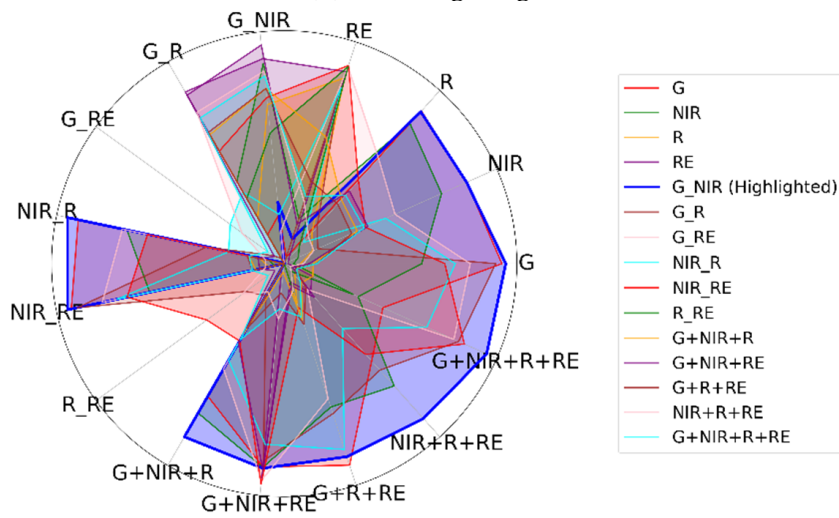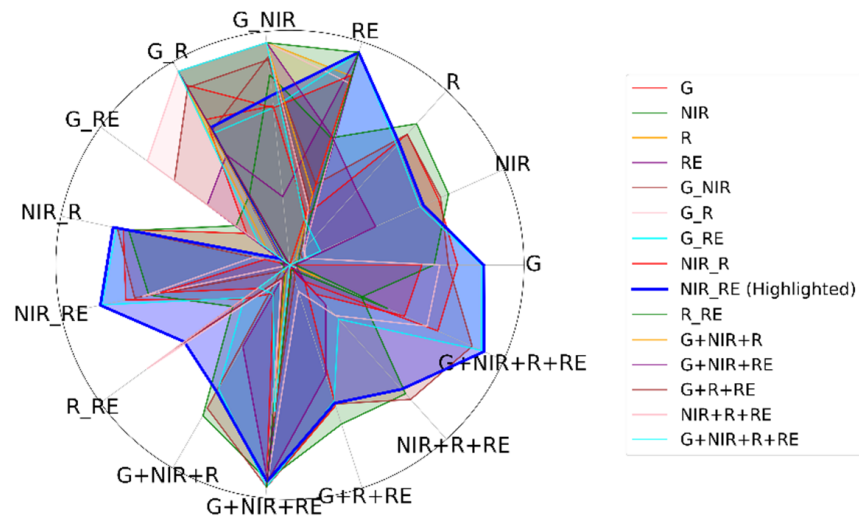

(**b**) Pre-Jointing Stage
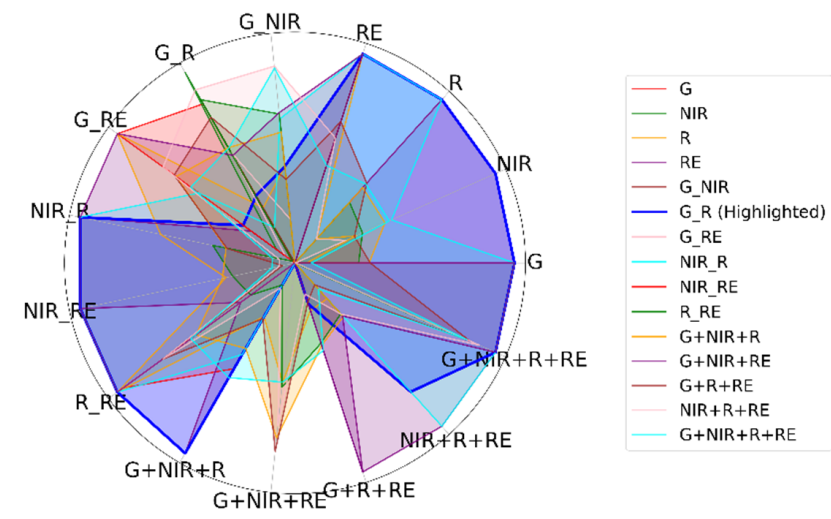
(**c**) Jointing Stage

Figure 4. *Cont.*

(**d**) Post-Jointing Stage

(**e**) Booting Stage

(**f**) Flowering Stage

Figure 4. *Cont.*

(**g**) Ripening Stage
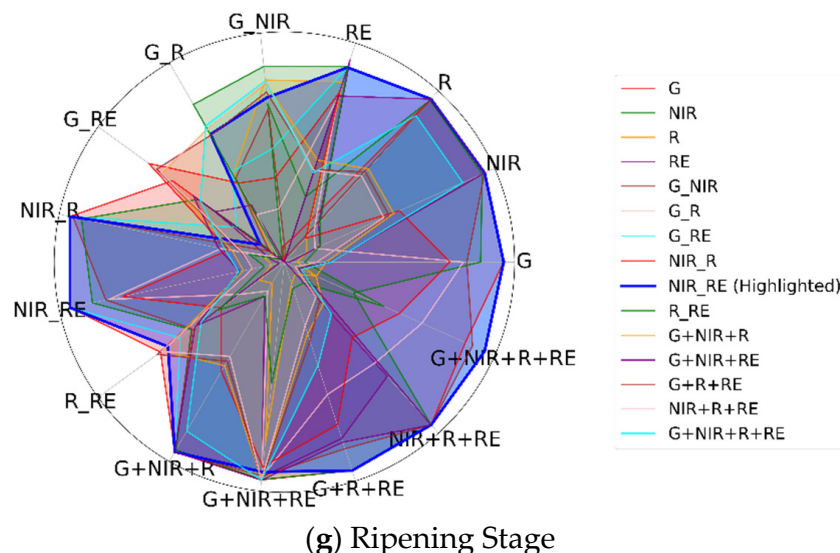
Figure 4. Radar chart of key spectral band features for remote-sensing identification of wheat growth stages. (**a**) Tillering Stage: The canopy coverage is relatively low, with the G band's mean value stabilizing at 0.65 and variance approximately 0.05, reflecting low canopy activity characteristics. (**b**) Pre-Jointing Stage: Canopy coverage increases significantly, with the G + NIR band's root-mean-square (RMS) value reaching 0.70, indicating a significant improvement in chlorophyll concentration and canopy density. (**c**) Jointing Stage: Canopy structure becomes complex, with the NIR band entropy reaching a peak of 1.2, reflecting a significant increase in plant texture complexity. (**d**) Post-Jointing Stage: Canopy activity stabilizes, but canopy fluctuations increase. The variance of the NIR + R band peaks at 0.12, indicating increased canopy variability. (**e**) Booting Stage: Canopy activity strengthens, with the energy value of the G + NIR band reaching 0.90, demonstrating strong concentration in canopy spectral reflectance. (**f**) Flowering Stage: Canopy coverage reaches its maximum, with the brightness concentration of the G + R + RE band combination peaking at 0.75, reflecting maximum canopy uniformity and reflectivity. (**g**) Ripening Stage: Canopy activity declines, and the median brightness of the NIR + R + RE band combination drops to 0.55, indicating a reduction in canopy reflectance intensity.

(1)   Tillering Stage: Canopy coverage is relatively low during this stage, and the NIR band is most sensitive to vegetation activity changes. The mean value is maintained between 0.60 and 0.70, while the variance is stable around 0.05. During this stage, vegetation reflectance is low and texture characteristics are simple, indicating that tillers have not fully developed, and the canopy has not yet formed a high-density coverage. Therefore, the spectral characteristics of the NIR band can effectively identify the low-activity state of the tillering canopy, making it an important basis for monitoring this stage.

(2)   Pre-Jointing Stage: This is a transitional stage from Tillering to Jointing, during which canopy coverage increases significantly. The Root-Mean-Square (RMS) value of the G + NIR combination rapidly rises to about 0.70, indicating a significant increase in chlorophyll concentration and canopy density. The G band reflects enhanced spectral reflectance of canopy leaves, while the NIR band captures the trend of canopy structural changes. The combination of these two bands can accurately distinguish the spectral characteristics of the Pre-Jointing stage, making it the core monitoring method for this period.

(3)   Jointing Stage: This stage marks a critical turning point in wheat growth, characterized by a significant increase in canopy structural complexity. The entropy value of the G + R combination peaks during this stage (approximately 1.2). Entropy reflects the complexity of canopy texture, while the G band is highly sensitive to vegetation

growth status and canopy health. During this stage, canopy coverage increases rapidly, spectral uniformity decreases, and texture complexity intensifies. The peak entropy value during this period makes it a key feature for distinguishing the jointing stage.

(4) Post-Jointing Stage: In this stage, wheat plants have completed jointing, and canopy activity tends to stabilize, although texture fluctuations increase. The variance of the G + R + RE combination peaks during this stage (approximately 0.12), reflecting possible stress conditions and canopy fluctuations. The G band captures changes in leaf physiological health, while the R and RE bands are sensitive to leaf aging and stress responses. The combination of these bands can effectively identify the canopy state characteristics of the Post-Jointing stage.

(5) Booting Stage: This is a vigorous growth period during which canopy activity further strengthens, while texture features tend to stabilize. The energy of the NIR + RE combination reaches its maximum value (approximately 0.90) during this stage, reflecting the concentration and uniformity of canopy spectral reflectance. The NIR band indicates high chlorophyll content, while the RE band captures further increases in canopy density. The peak energy value makes this metric an important basis for distinguishing the Booting stage.

(6) Flowering Stage: During this stage, canopy coverage reaches its peak, and spectral and texture features exhibit high uniformity and reflectivity. The Brightness Concentration of the NIR + RE combination peaks at approximately 0.75, reflecting the highest levels of canopy reflectance intensity and uniformity. The NIR band indicates chlorophyll activity, the RE band captures canopy health features, and the RE band is sensitive to nitrogen absorption during the Flowering stage, making it an effective method for precise identification of this stage.

(7) Ripening Stage: During the Ripening stage, canopy activity decreases significantly, spectral characteristics stabilize, and leaf aging becomes apparent. The median brightness of the NIR + RE combination drops to approximately 0.55, indicating a decline in canopy reflectance intensity. The NIR band captures the decline in canopy water content and health, the R band highlights the spectral characteristics of leaf aging, and the RE band reflects stable nitrogen absorption. Multi-band combinations enable precise identification of vegetation states during the Ripening stage.

3.3. Spectral Band Mapping for Different Growth Stages of Wheat

The practical impact of the model lies in its ability to provide real-time, high-resolution monitoring of wheat growth stages, health, and stress conditions through UAV-based multispectral remote sensing (Figure 5). This model can significantly improve precision agriculture by enabling early detection of diseases, water stress, and nutrient deficiencies, allowing for timely interventions. Additionally, the insights provided by the model can assist in optimizing agricultural practices such as irrigation, fertilization, and pest control, leading to more efficient use of resources, increased crop yields, and reduced environmental impact. By offering actionable data for informed decision-making, the model contributes to enhancing the sustainability and productivity of agricultural systems.

Based on the key characteristic bands or band combinations selected for different growth stages of wheat (e.g., G, NIR, RE, and their combinations), mapping analysis was conducted for the seven critical growth stages of wheat [49]. The selection of characteristic bands is rooted in growth characteristics such as canopy coverage, leaf spectral reflectance properties, and texture complexity at each growth stage. These features not only reflect the optical response changes of wheat during growth but also reveal plant health and growth patterns through spatial-spectral characteristics [42]. Mapping provides a visual

representation of the spectral reflection patterns of wheat at different growth stages, offering scientific insights for assessing plant growth status.

Multispectral sensors mounted on UAVs were employed to capture images during the seven typical growth stages [10]. By integrating the selected characteristic bands, quantitative identification of different growth stages was achieved. G band: Sensitive to canopy leaf activity, it reflects changes in chlorophyll concentration. NIR band: Captures canopy structural features and physiological health status. RE band: Strongly indicates nitrogen absorption and leaf maturity. R band: Highly sensitive to leaf aging and stress responses [35]. Quantitative extraction and mapping analysis of spectral reflection features for each growth stage reveal dynamic changes in canopy activity, plant health, and texture complexity throughout the wheat growth process. This approach provides a clear and scientific basis for evaluating the growth status of wheat plants [50].
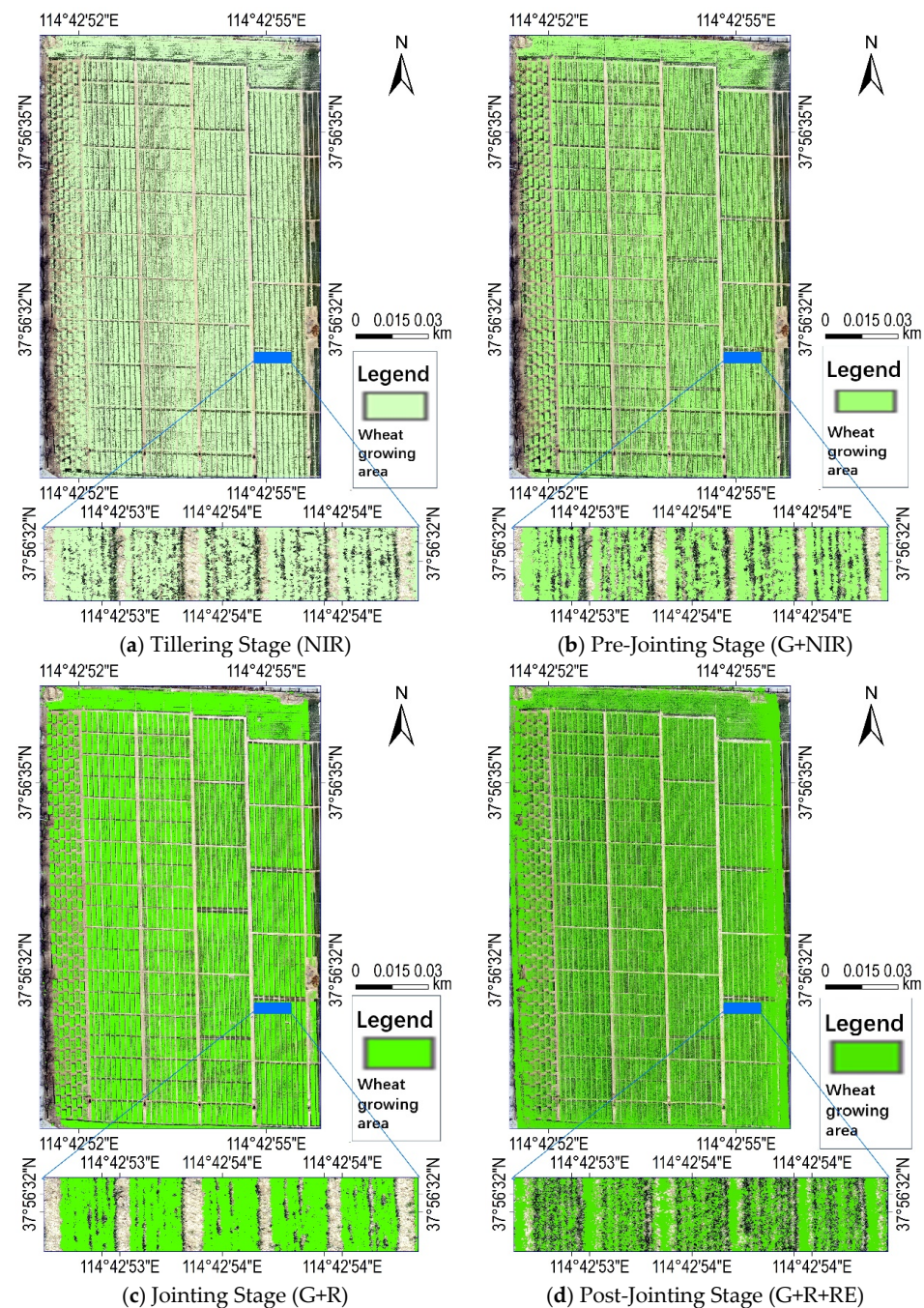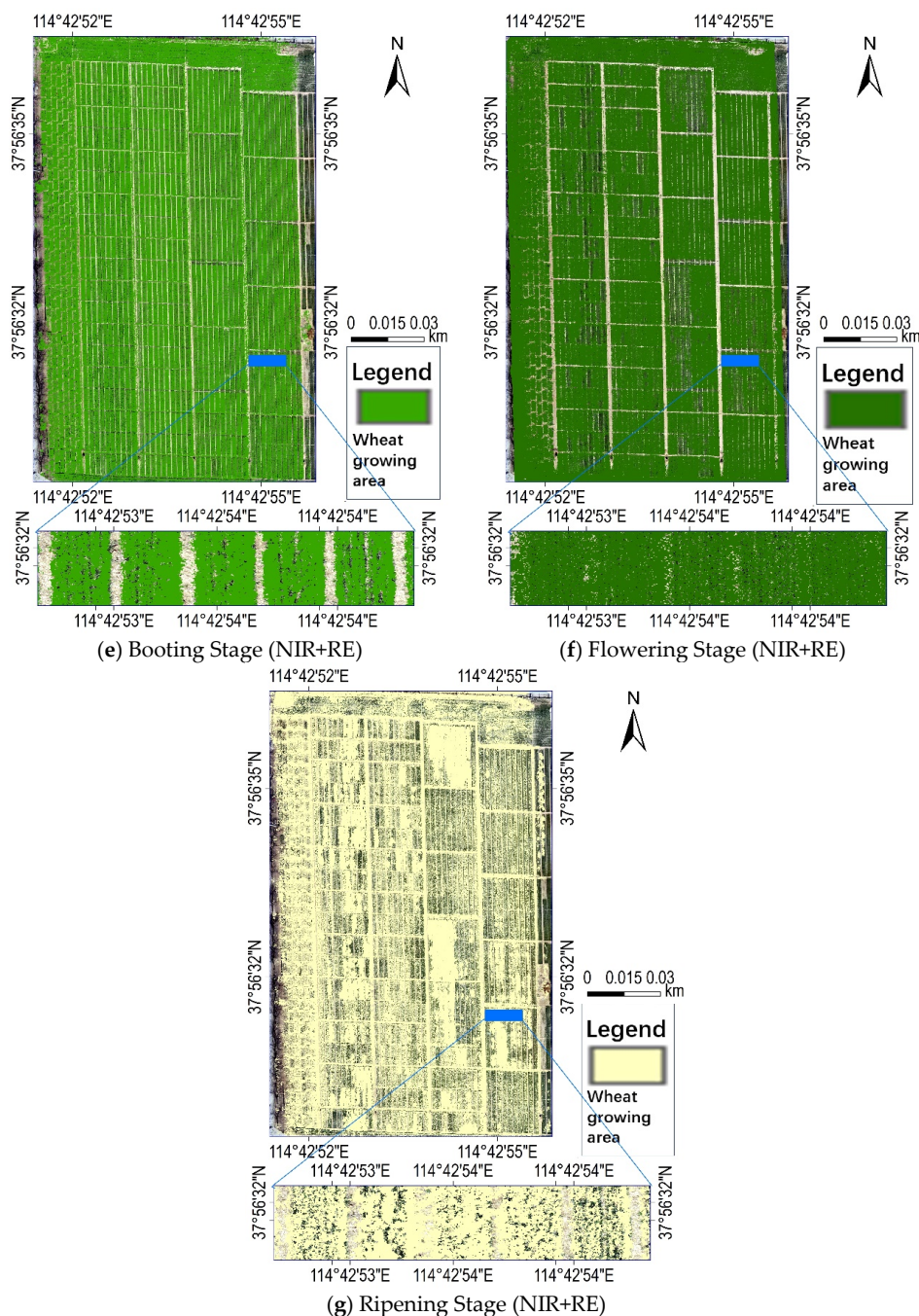

(**a**) Tillering Stage (NIR)

(**b**) Pre-Jointing Stage (G+NIR)

(**c**) Jointing Stage (G+R)

(**d**) Post-Jointing Stage (G+R+RE)

Figure 5. *Cont.*

(e) Booting Stage (NIR+RE)

(f) Flowering Stage (NIR+RE)

(g) Ripening Stage (NIR+RE)

Figure 5. Spectral mapping atlas of wheat characteristic bands at different growth stages. (**a**) Tillering Stage: Dominated by the G band, reflecting low canopy coverage and weak vegetation activity. Spectral differences between regions are minimal, indicating uniform low activity across the area. (**b**) Pre-Jointing Stage: The G + NIR band combination shows rapid increases in canopy coverage and significant enhancement in plant activity. Localized differences start to emerge, indicating uneven growth within the region. (**c**) Jointing Stage: The NIR band highlights increased canopy complexity, with distinct regional textures. The areas with peak entropy values correspond to zones of active growth. (**d**) Post-Jointing Stage: The NIR + R band combination emphasizes canopy variability, potentially indicating localized stress or physiological anomalies within the region. (**e**) Booting Stage: The G + NIR band combination presents high canopy density characteristics, with concentrated spectral energy reflecting this vigorous growth phase. (**f**) Flowering Stage: The G + R + RE band combination illustrates the maximum canopy coverage, with brightness-concentrated regions corresponding to healthy and active canopy zones. (**g**) Ripening Stage: The NIT + R + RE band combination reflects declining canopy activity, reduced spectral uniformity, and prominent signs of leaf aging, marking the final growth phase.

The implementation of UAV-based multispectral remote sensing in agricultural management can lead to significant cost reductions and increased operational efficiency. By minimizing the need for labor-intensive field surveys, this approach streamlines data collection, saving both time and resources. Additionally, the model's ability to accurately monitor crop health and detect stress or disease at early stages enables targeted interventions, such as optimized irrigation and fertilization, which reduces the overall use of resources. Early detection of crop issues also prevents potential yield losses and reduces the reliance on chemical treatments, leading to further cost savings and contributing to more sustainable and efficient farming practices.

4. Discussion

With the rapid development of precision agriculture, UAV remote-sensing technology has gained widespread attention for crop growth monitoring. Compared with traditional ground survey methods, UAV remote sensing provides refined and dynamic monitoring methods for crop growth processes through multispectral and high-resolution imagery [12,29]. Particularly in the full growth cycle of wheat, the canopy spectral reflectance characteristics and spatial texture properties exhibit significant spatiotemporal changes, revealing crop growth status, health levels, and stress conditions. By extracting key band or band combination features, remote sensing can quantitatively identify the growth characteristics of wheat at different growth stages [17]. The spatio-temporal data obtained from UAV imagery can be directly incorporated into GIS platforms for spatial analysis, allowing farmers and agronomists to visualize crop health, growth patterns, and field variability at a detailed level. This integration enables precise mapping of canopy conditions, which can be used to identify areas requiring targeted interventions, such as irrigation, fertilization, or pest control. Furthermore, the data can be linked to existing agricultural management systems, enhancing decision-making processes. By combining real-time spectral information with other farm management data, such as soil health, weather conditions, and historical crop performance, these systems can provide actionable insights for optimizing resource use, reducing waste, and improving crop yields. This integration of remote-sensing data with GIS and management systems can streamline agricultural practices, support precision farming strategies, and contribute to more sustainable and efficient agricultural operations. Combined with temporal analysis and spatial modeling, it offers a comprehensive monitoring solution for the entire growth cycle.

(1)   Technical Methods for Key Band Selection and Feature Extraction

The spectral characteristics of wheat exhibit significant dynamic changes at different growth stages, with specific bands or band combinations sensitively reflecting the physiological properties and growth conditions of the canopy. Multispectral sensors mounted on UAVs provide the data foundation for band selection and feature extraction through high spectral resolution acquisition [45]. During the tillering stage, the G band is a key band due to its sensitivity to chlorophyll activity, reflecting the low canopy coverage state. During the jointing stage, the NIR band captures the rapid increase in canopy structural complexity, representing texture complexity. During the Booting and Flowering stages, combinations such as G + NIR and G + R + RE accurately reveal plant health and spectral concentration. For these bands, UAV remote sensing employs multispectral mapping techniques based on band reflectance, combined with metrics such as mean value, entropy, and variance, to quantitatively extract and dynamically monitor the growth characteristics of wheat. Furthermore, band weight analysis using machine-learning algorithms (e.g., random forests or support vector machines) optimizes band combinations and improves the accuracy of growth stage classification. Technical discussions indicate that band selection and feature extraction are core elements of remote-sensing monitoring for wheat

growth stages, laying the theoretical and technical foundation for subsequent applications in precision agriculture [22,29,51].

(2)   Characteristics of Distribution and Precision Agriculture Management.

UAV remote sensing provides sub-meter spatial resolution, enabling detailed monitoring and analysis of wheat canopy characteristics at the field scale [35,47]. Through multispectral imagery and mapping with characteristic bands, the spatial distribution characteristics and uniformity of canopy coverage within fields can be reflected. For instance, during the post-jointing stage, the variance of the NIR + R band highlights localized anomalous areas, suggesting potential water stress or disease occurrences. During the flowering stage, regions with high brightness concentration in the G + R + RE band correspond to fields with good canopy health. These spatial distribution characteristics support precision agriculture management decisions, including precision fertilization, differential irrigation, and early pest and disease monitoring. Furthermore, combining UAV remote sensing with spatial analysis methods (e.g., NDVI-based zonal management or clustering analysis) enables hierarchical management within fields, improving resource utilization efficiency [46,52]. Additionally, with the integration of remote-sensing technology and geographic information systems (GIS), spatiotemporal dynamic models can be established to quantify the variation process of growth spatial distribution, providing data support for real-time diagnosis of crop health and production planning [44].

(3)   Monitoring over Time and Modeling the Growth Cycle.

The high-frequency monitoring capability of UAV remote sensing allows the entire growth cycle of wheat, from tillering to maturity, to be continuously recorded and analyzed. In the temporal dimension, spectral data reflect the key processes of plant growth [9,29,52]. For example, from the Tillering to Jointing stages, the reflectance of the G band increases significantly, reflecting an increase in chlorophyll content, while the entropy of the NIR band peaks during the jointing stage, revealing the turning point of canopy complexity. Extracting spectral characteristics over time can identify growth inflection points and critical stages of wheat. Further temporal modeling, such as dynamic NDVI curve fitting or biomass modeling based on remote-sensing features, provides a basis for predicting growth trends and yield estimation. Temporal monitoring can also identify abnormal growth phenomena, such as localized spectral anomalies during the flowering stage, which may indicate early signals of disease or stress. This dynamic monitoring capability in the temporal dimension advances agricultural monitoring from static description to dynamic modeling, laying a foundation for scientific management throughout the agricultural production cycle [39].

(4)   Technical Limitations and Future Development Directions

Although UAV remote sensing demonstrates significant advantages in extracting wheat growth stage information, it still has certain limitations. In terms of spatial resolution, although UAVs can provide high-resolution imagery, field heterogeneity may cause localized data biases [41,53]. In the temporal dimension, weather conditions (e.g., cloudy or rainy days) may affect multi-temporal data acquisition, resulting in discontinuity in temporal data. Additionally, the diversity of band selection and the complexity of data processing pose higher demands on algorithm design and computational resources. To address these issues, future development directions should include: integrating ground-based, UAV, and satellite remote-sensing data to build multi-scale fusion models for comprehensive spatiotemporal monitoring; introducing deep-learning technologies to enhance the accuracy of growth stage identification through feature extraction from hyperspectral data; optimizing data acquisition processes to improve the automation and intelligence of remote-sensing

monitoring; and developing open agricultural remote-sensing analysis platforms to promote technology dissemination and application in precision agriculture [20,54]. Through these advancements, UAV remote sensing will further drive the digital transformation of agricultural production, enabling efficient monitoring and management of crop growth.

In recent years, drones have become increasingly important in precision agriculture, offering a cost-effective and efficient solution for high-resolution crop monitoring. UAV technology has revolutionized how we gather spatial and temporal data on crops, allowing for detailed analysis of canopy health, growth dynamics, and environmental stressors. Recent reviews have highlighted the advantages of drones, including their flexibility, low operational costs, and ability to cover large areas with high spatial resolution. As a result, drones are increasingly integrated into crop management systems, helping farmers make more informed decisions regarding irrigation, fertilization, and pest control.

However, despite their advantages, the use of UAVs in agriculture is not without limitations. Key challenges include flight operating conditions such as weather, altitude, and flight time, which can affect the quality and consistency of the data collected. For example, adverse weather conditions like strong winds or precipitation can hinder flight stability, leading to incomplete or inaccurate data. Similarly, the operational altitude of UAVs can limit their coverage area, while the flight time is often constrained by battery life, requiring careful planning for large-scale field surveys. These factors must be considered when employing drones in precision agriculture to ensure optimal data collection and analysis. One limitation of this study is that the data were collected over a single year (March–June 2024). While the results provide valuable insights into wheat growth and the effectiveness of UAV remote sensing for precision agriculture, the findings may not fully account for interannual variability due to factors such as climate, soil conditions, and management practices. To improve the robustness and generalizability of the results, future studies should consider the use of multiyear data to assess the consistency of the observed trends and further validate the applicability of these methods across different environmental conditions.

The study was conducted in a single region with wheat as the focus crop, which may limit the broader applicability of the results to other regions or crops. While the findings provide valuable insights into the dynamic spectral characteristics of wheat across different growth stages, future research should expand to include diverse geographic regions and a variety of crop types. This would allow for a more comprehensive understanding of the temporal and spatial dynamics of canopy spectral features, thus improving the generalizability of UAV-based multispectral remote sensing techniques. By extending the scope of the study, the effectiveness of the monitoring framework could be evaluated across different environmental conditions and crop systems, offering valuable information for precision agriculture on a global scale.

5. Conclusions

This study, conducted at the Wheat Experimental Base of the Hebei Academy of Agriculture and Forestry Sciences, systematically analyzed the canopy spectral characteristics of wheat across seven critical growth stages using UAV-based multispectral remote sensing technology. By employing four spectral bands—G, R, RE, and NIR—and their combinations, this study mapped and quantified wheat growth states and health features during different growth stages [6,43]. The results revealed that the key spectral bands are highly sensitive to dynamic changes in the wheat canopy at various stages of wheat growth. For example, the G band highlighted low canopy coverage during the tillering stage, the NIR band showed significant increases in canopy structural complexity during the jointing stage, and the G + NIR combination reflected enhanced canopy density and concentrated spectral energy

during the booting stage [7,34]. Through band mapping, temporal analysis, and spatial distribution modeling, this study comprehensively demonstrated the spectral reflection dynamics and health conditions of wheat during its growth process. The findings indicate that multi-band combinations effectively enhance monitoring accuracy and information extraction efficiency, providing reliable technical means for full-cycle monitoring of wheat growth. Temporal monitoring identified critical growth inflection points and dynamic features, while spatial modeling offered targeted zonal decision-making support for precision agricultural management [12].

This research provides a scientific basis for precision agricultural management of wheat, achieving high-accuracy monitoring across the entire growth cycle and offering data support for disease warning, resource optimization, and yield improvement in agricultural production. Future efforts should focus on integrating ground-based observations and hyperspectral technology to build multi-source remote-sensing data-fusion models, further promoting the application and development of agricultural remote-sensing technology on a broader scale.

Author Contributions: D.Z.: methodology, software, and writing—original draft; L.H.: methodology, software, writing—original draft, project administration, and funding acquisition; L.L.: conceptualization, writing—review and editing, project administration, and funding acquisition; H.Q. and H.S.: investigation, data curation, and visualization; X.Z. and S.L.: writing—review and editing, supervision, and project administration; J.M., Y.L. (Yanwen Liu), Y.T. and Y.L. (Yao Liao): data curation, writing—review and editing, visualization, and software. All authors have read and agreed to the published version of the manuscript.

Institutional Review Board Statement: Not applicable.

Data Availability Statement: The data and algorithm code presented in this study are available on request from the corresponding author.

Conflicts of Interest: The authors declare no conflicts of interest.

Abbreviations

NDVI	Normalized Difference Vegetation Index
CI	Chlorophyll Index
G	Green Band
NIR	Near Infrared Band
R	Red Band
RE	Red Edge Band
VA	Variance
SD	Standard Deviation
EN	Entropy
SK	Skewness
KU	Kurtosis
BR	Brightness Range
RM	Root Mean Square

BC	Brightness Concentration
CO	Contrast
TV	Texture Variance
FE	Frequency Entropy
MA	Mean Absolute Deviation
EG	Energy
MB	Median Brightness

References

1. Maulit, A.; Nugumanova, A.; Apayev, K.; Baiburin, Y.; Sutula, M. A Multispectral UAV Imagery Dataset of Wheat, Soybean and Barley Crops in East Kazakhstan. *Data* **2023**, *8*, 88. [CrossRef]

2. Su, X.; Nian, Y.; Shaghaleh, H.; Hamad, A.; Yue, H.; Zhu, Y.; Li, J.; Wang, W.; Wang, H.; Ma, Q.; et al. Combining features selection strategy and features fusion strategy for SPAD estimation of winter wheat based on UAV multispectral imagery. *Front. Plant Sci.* **2024**, *15*, 1404238. [CrossRef] [PubMed]

3. Wang, Y.; Tan, S.; Jia, X.; Qi, L.; Liu, S.; Lu, H.; Wang, C.; Liu, W.; Zhao, X.; He, L.; et al. Estimating Relative Chlorophyll Content in Rice Leaves Using Unmanned Aerial Vehicle Multi-Spectral Images and Spectral-Textural Analysis. *Agronomy* **2023**, *13*, 1541. [CrossRef]

4. Mohammadi, S.; Uhlen, A.K.; Lillemo, M.; Ergon, A.; Shafiee, S. Enhancing phenotyping efficiency in faba bean breeding: Integrating UAV imaging and machine learning. *Precis. Agric.* **2024**, *25*, 1502–1528. [CrossRef]

5. Li, X.; Ba, Y.; Zhang, M.; Nong, M.; Yang, C.; Zhang, S. Sugarcane Nitrogen Concentration and Irrigation Level Prediction Based on UAV Multispectral Imagery. *Sensors* **2022**, *22*, 2711. [CrossRef]

6. Bian, C.; Shi, H.; Wu, S.; Zhang, K.; Wei, M.; Zhao, Y.; Sun, Y.; Zhuang, H.; Zhang, X.; Chen, S. Prediction of Field-Scale Wheat Yield Using Machine Learning Method and Multi-Spectral UAV Data. *Remote Sens.* **2022**, *14*, 1474. [CrossRef]

7. Shafi, U.; Mumtaz, R.; Anwar, Z.; Ajmal, M.M.; Khan, M.A.; Mahmood, Z.; Qamar, M.; Jhanzab, H.M. Tackling Food Insecurity Using Remote Sensing and Machine Learning-Based Crop Yield Prediction. *IEEE Access* **2023**, *11*, 108640–108657. [CrossRef]

8. Wilke, N.; Siegmann, B.; Postma, J.A.; Muller, O.; Krieger, V.; Pude, R.; Rascher, U. Assessment of plant density for barley and wheat using UAV multispectral imagery for high-throughput field phenotyping. *Comput. Electron. Agric.* **2021**, *189*, 106380. [CrossRef]

9. Fei, S.; Hassan, M.A.; Ma, Y.; Shu, M.; Cheng, Q.; Li, Z.; Chen, Z.; Xiao, Y. Entropy Weight Ensemble Framework for Yield Prediction of Winter Wheat Under Different Water Stress Treatments Using Unmanned Aerial Vehicle-Based Multispectral and Thermal Data. *Front. Plant Sci.* **2021**, *12*, 730181. [CrossRef] [PubMed]

10. Zhang, B.; Gu, L.; Dai, M.; Bao, X.; Sun, Q.; Zhang, M.; Qu, X.; Li, Z.; Zhen, W.; Gu, X. Estimation of grain filling rate of winter wheat using leaf chlorophyll and LAI extracted from UAV images. *Field Crops Res.* **2024**, *306*, 109198. [CrossRef]

11. Zhou, L.; Nie, C.; Su, T.; Xu, X.; Song, Y.; Yin, D.; Liu, S.; Liu, Y.; Bai, Y.; Jia, X.; et al. Evaluating the Canopy Chlorophyll Density of Maize at the Whole Growth Stage Based on Multi-Scale UAV Image Feature Fusion and Machine Learning Methods. *Agriculture* **2023**, *13*, 895. [CrossRef]

12. Shafiee, S.; Mroz, T.; Burud, I.; Lillemo, M. Evaluation of UAV multispectral cameras for yield and biomass prediction in wheat under different sun elevation angles and phenological stages. *Comput. Electron. Agric.* **2023**, *210*, 107874. [CrossRef]

13. Selvaraj, M.G.; Valderrama, M.; Guzman, D.; Valencia, M.; Ruiz, H.; Acharjee, A. Machine learning for high-throughput field phenotyping and image processing provides insight into the association of above and below-ground traits in cassava (*Manihot esculenta* Crantz). *Plant Methods* **2020**, *16*, 87. [CrossRef]

14. Jiang, J.; Zhang, Z.; Cao, Q.; Liang, Y.; Krienke, B.; Tian, Y.; Zhu, Y.; Cao, W.; Liu, X. Use of an Active Canopy Sensor Mounted on an Unmanned Aerial Vehicle to Monitor the Growth and Nitrogen Status of Winter Wheat. *Remote Sens.* **2020**, *12*, 3684. [CrossRef]

15. Fu, Z.; Jiang, J.; Gao, Y.; Krienke, B.; Wang, M.; Zhong, K.; Cao, Q.; Tian, Y.; Zhu, Y.; Cao, W.; et al. Wheat Growth Monitoring and Yield Estimation based on Multi-Rotor Unmanned Aerial Vehicle. *Remote Sens.* **2020**, *12*, 508. [CrossRef]

16. Dhakal, R.; Maimaitijiang, M.; Chang, J.; Caffe, M. Utilizing Spectral, Structural and Textural Features for Estimating Oat Above-Ground Biomass Using UAV-Based Multispectral Data and Machine Learning. *Sensors* **2023**, *23*, 9708. [CrossRef] [PubMed]

17. Prey, L.; Hanemann, A.; Ramgraber, L.; Seidl-Schulz, J.; Noack, P.O. UAV-Based Estimation of Grain Yield for Plant Breeding: Applied Strategies for Optimizing the Use of Sensors, Vegetation Indices, Growth Stages, and Machine Learning Algorithms. *Remote Sens.* **2022**, *14*, 6345. [CrossRef]

18. Liu, S.; Bai, X.; Zhu, G.; Zhang, Y.; Li, L.; Ren, T.; Lu, J. Remote estimation of leaf nitrogen concentration in winter oilseed rape across growth stages and seasons by correcting for the canopy structural effect. *Remote Sens. Environ.* **2023**, *284*, 113348. [CrossRef]

19. Camenzind, M.P.; Yu, K. Multi temporal multispectral UAV remote sensing allows for yield assessment across European wheat varieties already before flowering. *Front. Plant Sci.* **2024**, *14*, 1214931. [CrossRef] [PubMed]

20. Zhang, S.; Zhao, G.; Lang, K.; Su, B.; Chen, X.; Xi, X.; Zhang, H. Integrated Satellite, Unmanned Aerial Vehicle (UAV) and Ground Inversion of the SPAD of Winter Wheat in the Reviving Stage. *Sensors* **2019**, *19*, 1485. [CrossRef]

21. Wan, L.; Cen, H.; Zhu, J.; Zhang, J.; Zhu, Y.; Sun, D.; Du, X.; Zhai, L.; Weng, H.; Li, Y.; et al. Grain yield prediction of rice using multi-temporal UAV-based RGB and multispectral images and model transfer - a case study of small farmlands in the South of China. *Agric. For. Meteorol.* **2020**, *291*, 108096. [CrossRef]

22. Wang, S.; Tao, S.; Li, Y.; Wang, W. Leaf area index inversion of winter wheat based on UAV multispectral imagery. In Proceedings of the 2023 4th International Conference on Geology, Mapping and Remote Sensing (ICGMRS 2023), Wuhan, China, 14–16 April 2023; Volume 12978. [CrossRef]

23. Banerjee, B.P.; Sharma, V.; Spangenberg, G.; Kant, S. Machine Learning Regression Analysis for Estimation of Crop Emergence Using Multispectral UAV Imagery. *Remote Sens.* **2021**, *13*, 2918. [CrossRef]

24. Furlanetto, J.; Dal Ferro, N.; Caceffo, D.; Morari, F. Mapping hailstorm damage on winter wheat (*Triticum aestivum* L.) using a microscale UAV hyperspectral approach. *Precis. Agric.* **2024**, *25*, 681–703. [CrossRef]

25. Ferro, M.V.; Sørensen, C.G.; Catania, P. Comparison of different computer vision methods for vineyard canopy detection using UAV multispectral images. *Comput. Electron. Agric.* **2024**, *225*, 109277. [CrossRef]

26. Shu, M.; Fei, S.; Zhang, B.; Yang, X.; Guo, Y.; Li, B.; Ma, Y. Application of UAV Multisensor Data and Ensemble Approach for High-Throughput Estimation of Maize Phenotyping Traits. *Plant Phenomics* **2022**, *2022*, 9802585. [CrossRef]

27. Zhang, S.-H.; He, L.; Duan, J.-Z.; Zang, S.-L.; Yang, T.-C.; Schulthess, U.R.S.; Guo, T.-C.; Wang, C.-Y.; Feng, W. Aboveground wheat biomass estimation from a low-altitude UAV platform based on multimodal remote sensing data fusion with the introduction of terrain factors. *Precis. Agric.* **2024**, *25*, 119–145. [CrossRef]

28. Yang, Q.; Shi, L.; Han, J.; Chen, Z.; Yu, J. A VI-based phenology adaptation approach for rice crop monitoring using UAV multispectral images. *Field Crops Res.* **2022**, *277*, 108419. [CrossRef]

29. Heinemann, P.; Haug, S.; Schmidhalter, U. Evaluating and defining agronomically relevant detection limits for spectral reflectance-based assessment of N uptake in wheat. *Eur. J. Agron.* **2022**, *140*, 126609. [CrossRef]

30. Wang, J.; Lou, Y.; Wang, W.; Liu, S.; Zhang, H.; Hui, X.; Wang, Y.; Yan, H.; Maes, W.H. A robust model for diagnosing water stress of winter wheat by combining UAV multispectral and thermal remote sensing. *Agric. Water Manag.* **2024**, *291*, 108616. [CrossRef]

31. Qiao, L.; Tang, W.; Gao, D.; Zhao, R.; An, L.; Li, M.; Sun, H.; Song, D. UAV-based chlorophyll content estimation by evaluating vegetation index responses under different crop coverages. *Comput. Electron. Agric.* **2022**, *196*, 106775. [CrossRef]

32. Fu, Z.; Yu, S.; Zhang, J.; Xi, H.; Gao, Y.; Lu, R.; Zheng, H.; Zhu, Y.; Cao, W.; Liu, X. Combining UAV multispectral imagery and ecological factors to estimate leaf nitrogen and grain protein content of wheat. *Eur. J. Agron.* **2022**, *132*, 126405. [CrossRef]

33. Zhang, Y.; Han, W.; Niu, X.; Li, G. Maize Crop Coefficient Estimated from UAV-Measured Multispectral Vegetation Indices. *Sensors* **2019**, *19*, 5250. [CrossRef]

34. Revill, A.; Florence, A.; MacArthur, A.; Hoad, S.; Rees, R.; Williams, M. Quantifying Uncertainty and Bridging the Scaling Gap in the Retrieval of Leaf Area Index by Coupling Sentinel-2 and UAV Observations. *Remote Sens.* **2020**, *12*, 1843. [CrossRef]

35. Wu, Q.; Zhang, Y.; Zhao, Z.; Xie, M.; Hou, D. Estimation of Relative Chlorophyll Content in Spring Wheat Based on Multi-Temporal UAV Remote Sensing. *Agronomy* **2023**, *13*, 211. [CrossRef]

36. Su, J.; Liu, C.; Hu, X.; Xu, X.; Guo, L.; Chen, W.-H. Spatio-temporal monitoring of wheat yellow rust using UAV multispectral imagery. *Comput. Electron. Agric.* **2019**, *167*, 105035. [CrossRef]

37. Wei, L.; Yang, H.; Niu, Y.; Zhang, Y.; Xu, L.; Chai, X. Wheat biomass, yield, and straw-grain ratio estimation from multi-temporal UAV-based RGB and multispectral images. *Biosyst. Eng.* **2023**, *234*, 187–205. [CrossRef]

38. Zheng, H.; Ma, J.; Zhou, M.; Li, D.; Yao, X.; Cao, W.; Zhu, Y.; Cheng, T. Enhancing the Nitrogen Signals of Rice Canopies across Critical Growth Stages through the Integration of Textural and Spectral Information from Unmanned Aerial Vehicle (UAV) Multispectral Imagery. *Remote Sens.* **2020**, *12*, 957. [CrossRef]

39. Liu, Y.; Liu, G.; Sun, H.; An, L.; Zhao, R.; Liu, M.; Tang, W.; Li, M.; Yan, X.; Ma, Y.; et al. Exploring multi-features in UAV based optical and thermal infrared images to estimate disease severity of wheat powdery mildew. *Comput. Electron. Agric.* **2024**, *225*, 109285. [CrossRef]

40. Zhou, H.; Yang, J.; Lou, W.; Sheng, L.; Li, D.; Hu, H. Improving grain yield prediction through fusion of multi-temporal spectral features and agronomic trait parameters derived from UAV imagery. *Front. Plant Sci.* **2023**, *14*, 1217448. [CrossRef] [PubMed]

41. Lu, R.; Zhang, P.; Fu, Z.; Jiang, J.; Wu, J.; Cao, Q.; Tian, Y.; Zhu, Y.; Cao, W.; Liu, X. Improving the spatial and temporal estimation of ecosystem respiration using multi-source data and machine learning methods in a rainfed winter wheat cropland. *Sci. Total Environ.* **2023**, *871*, 161967. [CrossRef]

42. Wang, F.; Yang, M.; Ma, L.; Zhang, T.; Qin, W.; Li, W.; Zhang, Y.; Sun, Z.; Wang, Z.; Li, F.; et al. Estimation of Above-Ground Biomass of Winter Wheat Based on Consumer-Grade Multi-Spectral UAV. *Remote Sens.* **2022**, *14*, 1251. [CrossRef]

43. Sanders, J.T.; Jones, E.A.L.; Minter, A.; Austin, R.; Roberson, G.T.; Richardson, R.J.; Everman, W.J. Remote Sensing for Italian Ryegrass [*Lolium perenne* L. ssp. multiflorum (Lam.) Husnot] Detection in Winter Wheat (*Triticum aestivum* L.). *Front. Agron.* **2021**, *3*, 687112. [CrossRef]

44. Jiang, J.; Atkinson, P.M.; Chen, C.; Cao, Q.; Tian, Y.; Zhu, Y.; Liu, X.; Cao, W. Combining UAV and Sentinel-2 satellite multi-spectral images to diagnose crop growth and N status in winter wheat at the county scale. *Field Crops Res.* **2023**, *294*, 108860. [CrossRef]

45. Wang, J.; Yin, Q.; Cao, L.; Zhang, Y.; Li, W.; Wang, W.; Zhou, G.; Huo, Z. Enhancing Winter Wheat Soil-Plant Analysis Development Value Prediction through Evaluating Unmanned Aerial Vehicle Flight Altitudes, Predictor Variable Combinations, and Machine Learning Algorithms. *Plants* **2024**, *13*, 1926. [CrossRef]

46. Li, X.; Su, X.; Li, J.; Anwar, S.; Zhu, X.; Ma, Q.; Wang, W.; Liu, J. Coupling Image-Fusion Techniques with Machine Learning to Enhance Dynamic Monitoring of Nitrogen Content in Winter Wheat from UAV Multi-Source. *Agriculture* **2024**, *14*, 1797. [CrossRef]

47. Zhang, B.; Chen, Y.; Liu, H.; Wu, Y.; Ye, S.; Yang, N.; Bai, X.; Huang, J.; Xie, P.; Zhang, Z.; et al. Monitoring soil moisture content in the root zone of winter wheat with multi-angle multispectral imagery. *Int. J. Remote Sens.* **2024**, *45*, 4692–4709. [CrossRef]

48. Wang, W.; Gao, X.; Cheng, Y.; Ren, Y.; Zhang, Z.; Wang, R.; Cao, J.; Geng, H. QTL Mapping of Leaf Area Index and Chlorophyll Content Based on UAV Remote Sensing in Wheat. *Agriculture* **2022**, *12*, 595. [CrossRef]

49. Zhang, X.; Zhang, K.; Wu, S.; Shi, H.; Sun, Y.; Zhao, Y.; Fu, E.; Chen, S.; Bian, C.; Ban, W. An Investigation of Winter Wheat Leaf Area Index Fitting Model Using Spectral and Canopy Height Model Data from Unmanned Aerial Vehicle Imagery. *Remote Sens.* **2022**, *14*, 5087. [CrossRef]

50. Yin, Q.; Zhang, Y.; Li, W.; Wang, J.; Wang, W.; Ahmad, I.; Zhou, G.; Huo, Z. Estimation of Winter Wheat SPAD Values Based on UAV Multispectral Remote Sensing. *Remote Sens.* **2023**, *15*, 3595. [CrossRef]

51. Chen, P.; Wang, F. Effect of crop spectra purification on plant nitrogen concentration estimations performed using high-spatial-resolution images obtained with unmanned aerial vehicles. *Field Crops Res.* **2022**, *288*, 108708. [CrossRef]

52. Hasan, U.; Sawut, M.; Chen, S. Estimating the Leaf Area Index of Winter Wheat Based on Unmanned Aerial Vehicle RGB-Image Parameters. *Sustainability* **2019**, *11*, 6829. [CrossRef]

53. Feng, W.; Lan, Y.; Zhao, H.; Tang, Z.; Peng, W.; Che, H.; Zhu, J. Identification of High-Photosynthetic-Efficiency Wheat Varieties Based on Multi-Source Remote Sensing from UAVs. *Agronomy* **2024**, *14*, 2389. [CrossRef]

54. Su, X.; Nian, Y.; Yue, H.; Zhu, Y.; Li, J.; Wang, W.; Sheng, Y.; Ma, Q.; Liu, J.; Wang, W.; et al. Improving Wheat Leaf Nitrogen Concentration (LNC) Estimation across Multiple Growth Stages Using Feature Combination Indices (FCIs) from UAV Multispectral Imagery. *Agronomy* **2024**, *14*, 1052. [CrossRef]